Desalination and Water Treatment 8 (2009) 68–90
www.deswater.com
1944-3994/1944-3986

Implications of critical flux and cake enhanced osmotic pressure (CEOP) on colloidal fouling in reverse osmosis: Modeling approach

T.H. Chong, A.G. Fane*

Singapore Membrane Technology Centre, Nanyang Technological University, 50 Nanyang Avenue, 639798 Singapore
Tel. +65 6790 5272; Fax +65 6791 0756; email: AGFane@ntu.edu.sg

Received 19 January 2009; accepted 28 July 2009

ABSTRACT

This article describes a predictive model to account for the performance of a reverse osmosis (RO) system under the influence of colloidal fouling (using silica particles as model colloids) in terms of transmembrane pressure increase ($\triangle$TMP) in constant flux operation or flux drop ($\triangle J_v$) in constant pressure operation. The predictive model considers the implications of both the critical flux (J_{crit}) and cake enhanced osmotic pressure (CEOP) phenomenon and is based on the membrane retention, concentration polarization, mass transfer, resistance in series and osmotic pressure model, cake resistance, and critical flux concept.

Keywords: Reverse osmosis; Colloidal fouling; Critical flux; Cake enhanced osmotic pressure (CEOP); Constant flux; Constant transmembrane pressure

1. Introduction

Conventionally, fouling models of reverse osmosis (RO) have not considered the simultaneous effects of critical flux (J_{crit}) and cake enhanced osmotic pressure (CEOP) and therefore suffered from a few disadvantages. Firstly, the models are not able to identify the initiation and intensity of fouling. Operating a RO system below the critical flux will prevent the deposition of colloidal particles on the membrane. On the other hand, if operated above the critical flux, the particles will start to deposit and form a cake layer. Hence, the accumulation of deposits on the membrane is controlled by the net flux, which is the difference between the operating flux, J_v and the critical flux, J_{crit}, or ($J_v - J_{crit}$). Subsequently, the build-up of this 'unstirred' deposit layer on the membrane surface will result in the CEOP phenomenon through the hindered back-diffusion of solutes [1]. Back-diffusion of retained solutes is hindered because the solutes now need to diffuse through the tortuous paths within the cake layer. The solutes in this ''unstirred'' deposit layer are not exposed to crossflow and the concentration and osmotic pressure at the membrane surface are greatly enhanced. The CEOP phenomenon concept is depicted in Fig. 1. In most of the previous studies, an increase in the transmembrane pressure (TMP) or decline in flux was attributed solely to the induced hydraulic resistance (R_f) of the deposit layer. However, the CEOP effect suggests a loss in the available effective driving force rather than an additional hydraulic resistance, R_f, as demonstrated in our previous work [2]. Neglecting the CEOP effect over-estimates the contribution of the cake resistance, or in other words it does not require a thick layer of cake to cause a significant increase in TMP or decline in flux. Therefore, a fouling model that incorporates both the critical flux and CEOP effects is essential for predicting the long-term performance of an RO membrane.

*Corresponding author

Presented at the First UK–Israeli Workshop and Research Event on the Application of Membrane Technology in Water Treatment and Desalination, 15–20 June 2008, University of Oxford, UK.

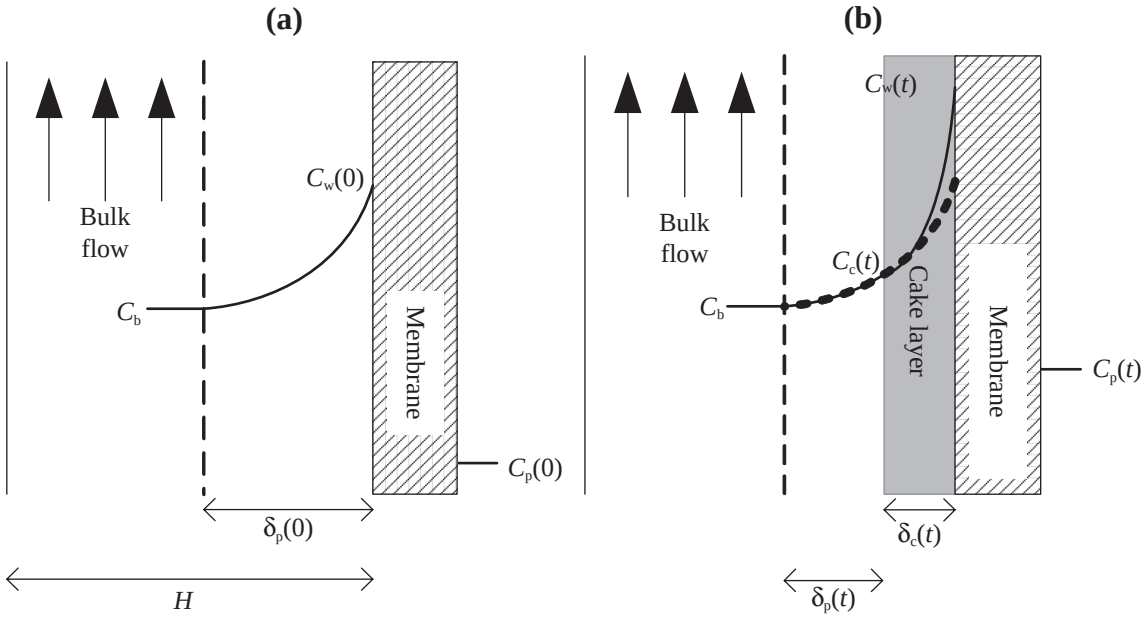

Fig. 1. Illustration of concentration profile and boundary layer in RO membrane at steady state (a) before fouling or $t = 0$, and (b) after fouling or $t = t$.

The focus of this modeling work is on the membrane performance at constant flux and constant pressure operation. To date, most of the work reported in literature considers the fouling process under fixed pressure conditions. However, both situations are important as in practice RO plants tend to be operated at fixed production rates, which requires constant flux. So typically TMP is adjusted to compensate for fouling. If this leads to operating at the maximum pump pressure, it may be necessary to allow the flux to decline. Therefore, it is essential to understand the fouling mechanism and the controlling parameters in both cases. The membrane performance loss can be evaluated in terms of transmembrane pressure increase ($\triangle$TMP) for constant flux operation or flux decline ($\triangle J_v$) in constant pressure operation. In the following analysis, a comparison of the relative contribution of CEOP and R_f on the performance loss is carried out. Colloidal silica particles are selected as the model compound in the simulation, as the data can be readily obtained from the results presented in our previous work [2].

2. Model development

The simple predictive model for colloidal fouling in RO developed in this study combines the equations for membrane retention, concentration polarization, mass transfer, resistance in series and osmotic pressure, cake resistance, and critical flux. The system considered in the model is illustrated in Fig. 1. The assumptions made in the model are:

(1) Non-compressible cake, e.g. specific cake resistance is independent of the pressure change. Colloidal silica cake was reported to be compressible [3]. However, under the high pressure of the RO process, the effect of time-dependent cake compressibility can be ignored.
(2) Physical properties (viscosity, density, and particle size) of solution and cake remain constant.
(3) Membrane properties (resistance and real retention) remain constant.
(4) The cake layer does not reject the solutes.

The model is presented in the following section.

2.1. Membrane retention

Membrane real retention, R_{real}, is an intrinsic property of a membrane and is assumed to remain constant; unlike the observed retention which is affected by the degree of concentration polarization and fouling. Hence, before fouling:

$$R_{real} = \frac{C_w(0) - C_p(0)}{C_w(0)}, \quad (1)$$

where C_w and C_p are the solute concentration at membrane wall and in permeate, respectively.

After fouling:

$$R_{\text{real}} = \frac{C_{\text{w}}(t) - C_{\text{p}}(t)}{C_{\text{w}}(t)}. \tag{2}$$

2.2. Concentration polarization

Concentration polarization (CP) is due to the accumulation of the rejected solutes on the membrane surface. The solutes diffuse back into the bulk solution due to the solute concentration gradient. For a clean membrane system, the steady state mass balance of solutes in the polarized layer is:

$$J_{\text{v}}(0)C - D\frac{\text{d}C}{\text{d}x} = J_{\text{v}}(0)C_{\text{p}}(0) \tag{3}$$

with the boundary conditions:

$x = 0; \quad C = C_{\text{b}}$

$x = \delta_{\text{p}}(0); \quad C = C_{\text{w}}(0)$

solving yields:

$$\begin{aligned}\text{CP}(0) &= \exp\left(\frac{J_{\text{v}}(0)}{D/\delta_{\text{p}}(0)}\right) = \exp\left(\frac{J_{\text{v}}(0)}{k_{\text{m}}(0)}\right)\\ &= \frac{C_{\text{w}}(0) - C_{\text{p}}(0)}{C_{\text{b}} - C_{\text{p}}(0)},\end{aligned} \tag{4}$$

where J_{v} is the flux, D is the diffusivity of solute, δ_{p} is the polarized layer thickness, k_{m} is the boundary layer mass transfer coefficient, and C_{b} is the bulk concentration. For a fouled membrane, the concentration at the wall builds up due to the CEOP effect. The mass balance of solutes in the polarized layer is:

$$J_{\text{v}}(t)\,C - D\frac{\text{d}C}{\text{d}x} = J_{\text{v}}(t)\,C_{\text{p}}(t) \tag{5}$$

with the boundary conditions:

$x = 0; \quad C = C_{\text{b}}$

$x = \delta_{\text{p}}(t); \quad C = C_{\text{c}}(t)$

solving yields:

$$\exp\left(\frac{J_{\text{v}}(t)}{D/\delta_{\text{p}}(t)}\right) = \exp\left(\frac{J_{\text{v}}(t)}{k_{\text{p}}(t)}\right) = \frac{C_{\text{c}}(t) - C_{\text{p}}(t)}{C_{\text{b}} - C_{\text{p}}(t)}, \tag{6}$$

where C_{c} is the solute concentration at the solution/cake interface and k_{p} is the mass transfer in the polarized layer. The mass balance of solutes in the cake layer is:

$$J_{\text{v}}(t)\,C - D_{\text{c}}(t)\frac{\text{d}C}{\text{d}x} = J_{\text{v}}(t)\,C_{\text{p}}(t) \tag{7}$$

with the boundary conditions:

$x = \delta_{\text{p}}(t); \quad C = C_{\text{c}}(t)$

$x = \delta_{\text{p}}(t) + \delta_{\text{c}}(t); \quad C = C_{\text{w}}(t)$

solving yields:

$$\exp\left(\frac{J_{\text{v}}(t)}{D_{\text{c}}(t)/\delta_{\text{c}}(t)}\right) = \exp\left(\frac{J_{\text{v}}(t)}{k_{\text{c}}(t)}\right) = \frac{C_{\text{w}}(t) - C_{\text{p}}(t)}{C_{\text{c}}(t) - C_{\text{p}}(t)}, \tag{8}$$

where D_{c} is the effective solute diffusivity in the cake layer, k_{c} is the mass transfer in the cake layer, δ_{c} is the cake layer thickness. By combining Eqs. (6) and (8):

$$\begin{aligned}&\exp\left(\frac{J_{\text{v}}(t)}{k_{\text{p}}(t)}\right)\exp\left(\frac{J_{\text{v}}(t)}{k_{\text{c}}(t)}\right)\\ &\qquad = \left(\frac{C_{\text{c}}(t) - C_{\text{p}}(t)}{C_{\text{b}} - C_{\text{p}}(t)}\right)\left(\frac{C_{\text{w}}(t) - C_{\text{p}}(t)}{C_{\text{c}}(t) - C_{\text{p}}(t)}\right) \text{ or}\end{aligned}$$

$$\begin{aligned}\text{CP}(t) &= \exp\left(\frac{J_{\text{v}}(t)}{k_{\text{p}}(t)} + \frac{J_{\text{v}}(t)}{k_{\text{c}}(t)}\right) = \exp\left(\frac{J_{\text{v}}(t)}{k_{\text{m}}(t)}\right)\\ &= \frac{C_{\text{w}}(t) - C_{\text{p}}(t)}{C_{\text{b}} - C_{\text{p}}(t)},\end{aligned} \tag{9}$$

where $k_{\text{m}}(t)$ is the effective mass transfer coefficient in a fouled channel, in which $1/k_{\text{m}} = 1/k_{\text{p}}(t) + 1/k_{\text{c}}(t)$.

2.3. Mass transfer

For a clean membrane system with a thin rectangular channel, the mass transfer coefficient for laminar flow from the Graetz–Lévêque correlation is [4]:

$$k_{\text{m}}(0) = 1.62\left(\frac{QD^2}{2W(H)^2L}\right)^{1/3} = 1.62\left(\frac{vD^2}{2HL}\right)^{1/3}, \tag{10}$$

where Q is the crossflow flow rate, W is the channel width, H is the channel height, L is the channel length, and v is the crossflow velocity. For a fouled system, the effective mass transfer comprises two parts; the mass transfer in the un-fouled section and the mass transfer in the cake layer. For the un-fouled section:

$$k_{\text{p}}(t) = \frac{D}{\delta_{\text{p}}(t)}. \tag{11}$$

Let us assume $\delta_c(t)$ is small as compared to the channel height, e.g. $\delta_c(t) \ll H$. This is a reasonable assumption as shown in our previous work [2], only a minute amount of cake was formed even at high flux and low crossflow velocity, and hence the channel height was not assumed to be altered by the cake layer. Therefore,

$$k_p(t) \approx \frac{D}{\delta_p(0)} = k_m(0). \tag{12}$$

The mass transfer in a cake layer is:

$$k_c(t) = \frac{D_c(t)}{\delta_c(t)}, \tag{13}$$

where $D_c(t)$ is the diffusion of solute in the porous cake layer with a tortuous path, and can be estimated by [5]:

$$D_c(t) = D\left(\frac{\varepsilon(t)}{1 - \ln \varepsilon(t)^2}\right), \tag{14}$$

where ε is the porosity of cake layer. Hence,

$$k_c(t) = \frac{D}{\delta_c(t)}\left(\frac{\varepsilon(t)}{1 - \ln \varepsilon(t)^2}\right). \tag{15}$$

Therefore, the overall mass transfer in a fouled channel is:

$$\frac{1}{k_m(t)} = \frac{1}{k_p(t)} + \frac{1}{k_c(t)} = \frac{1}{k_m(0)} + \frac{\delta_c(t)}{D}\left(\frac{1 - \ln \varepsilon(t)^2}{\varepsilon(t)}\right). \tag{16}$$

For constant flux operation, multiplying Eq. (16) by J_v and taking exponentials, yields:

$$\begin{aligned}\frac{CP(t)}{CP(0)} &= \exp\left\{\left(\frac{J_v}{k_m(t)}\right) - \left(\frac{J_v}{k_m(0)}\right)\right\} \\ &= \exp\left\{\frac{J_v \delta_c(t)}{D}\left(\frac{1 - \ln \varepsilon(t)^2}{\varepsilon(t)}\right)\right\}.\end{aligned} \tag{17}$$

Eq. (17) shows that the CP level in a fouled membrane system is strongly affected by the operating flux, cake layer thickness, and porosity as CP(t) is an exponential function of these parameters.

2.4. Resistance in series and osmotic pressure filtration equation

2.4.1. Constant flux operation

Before fouling occurs, the flux can be calculated from the filtration model:

$$J_v = \frac{TMP(0) - CP(0)\Delta\Pi_b(0)}{\mu R_m}, \tag{18}$$

where μ is the viscosity of the permeate, R_m is the intrinsic membrane resistance, and $\Delta\Pi_b$ is the osmotic pressure difference between the feed and permeate solutions. The osmotic pressure of sodium chloride at 25 °C can be estimated by [6]:

$$\log(\Pi_{NaCl}) = 0.9937 \log(C_{NaCl}) - 3.0797, \tag{19}$$

where C_{NaCl} is concentration of sodium chloride in ppm. For a fouled membrane, where there is an increase in TMP and CP, and build-up of cake resistance, R_f, the filtration equation can be written as:

$$J_v = \frac{TMP(t) - CP(t)\Delta\Pi_b(t)}{\mu(R_m + R_f(t))}. \tag{20}$$

Combining Eqs. (18) and (20), yields:

$$\left\{\frac{CP(t)\Delta\Pi_b(t) - CP(0)\Delta\Pi_b(0)}{TMP(t) - TMP(0)}\right\} + \left\{\frac{J_v \mu R_f(t)}{TMP(t) - TMP(0)}\right\} = 1. \tag{21}$$

The first and second terms on the left indicate the relative contribution of CEOP and R_f on the overall increase in the TMP.

2.4.2. Constant pressure operation

Before fouling starts, the TMP required for filtration is:

$$TMP = J_v(0)\mu R_m + CP(0)\Delta\Pi_b(0). \tag{22}$$

Fouling causes a drop in the flux, a build-up in the cake resistance and a change in the CP. Hence,

$$TMP = J_v(t)\mu(R_m + R_f(t)) + CP(t)\Delta\Pi_b(t). \tag{23}$$

Combining Eqs. (22) and (23), yields:

$$\left\{\frac{CP(t)\Delta\Pi_b(t) - CP(0)\Delta\Pi_b(0)}{(J_v(0) - J_v(t))\mu R_m}\right\} + \left\{\frac{J_v(t)\mu R_f(t)}{(J_v(0) - J_v(t))\mu R_m}\right\} = 1. \tag{24}$$

The first and second terms on the left indicate the relative contribution of CEOP and R_f on the flux decline, respectively.

2.5. Cake resistance and thickness

The hydraulic resistance of the cake, R_f, can be estimated by:

$$R_f(t) = \alpha_f(t) m_f(t), \tag{25}$$

where α_f is the specific cake resistance and m_f is the mass of deposit per unit area. The specific cake resistance, $\alpha_f(t)$ can be estimated from the Carmen–Kozeny equation [7]:

$$\alpha_f(t) = \frac{180(1 - \varepsilon(t))}{\rho_p d_p^2 \varepsilon(t)^3}, \tag{26}$$

where ρ_p and d_p are the particle density and diameter, respectively. As seen from Eq. (26), $\alpha_f \propto 1/{d_p}^2$, so a 10-fold increase in the particle size (e.g. from 20 to 200 nm) will cause a 100-fold decrease in the specific cake resistance. Also, $\alpha_f(t)$ is a function of ionic strength of the solution [3,8] and can be estimated by [9]:

$$\alpha_f(t) = 0.07127 \times 10^{15} (C_{NaCl})^{0.3384}. \tag{27}$$

The cake layer thickness can be estimated from the mass load:

$$\delta_c(t) = \frac{m_f(t)}{\rho_p(1 - \varepsilon(t))}. \tag{28}$$

2.6. Critical flux

The accumulation of the deposit layer on the membrane is related to the critical flux, J_{crit} [10] as well as the fractional deposition constant, Φ [9] via:

$$m_f(t) = \Phi C_{b,SiO_2}(J_v(t) - J_{crit})t, \tag{29}$$

where C_{b,SiO_2} is the bulk concentration of silica. For simplicity, all particles convected to the membrane surface due to permeation drag beyond the critical flux are assumed to fully deposit on the surface, and hence the fractional deposition constant, Φ, is assumed to be 1.0 in the above equation. However, this assumption is only correct at lower crossflow velocities [9]. In addition, J_{crit} is a function of the crossflow velocity, which is commonly expressed in the form of [11–13]:

$$J_{crit} = a \cdot v^b \tag{30}$$

For colloidal silica particles, the experimentally determined values of a and b are 47.5 and 0.395, respectively, at $d_p = 20$ nm [9]. The critical flux is also a function of the particle size, d_p, according to the particle transport mechanisms in crossflow filtration [14–16]. For simplicity, only two types of particle back-transport mechanism are considered here, Brownian and shear-induced diffusion. For sub-micron size particles (typically <0.1 μm), molecular or Brownian diffusion is important [17]. Shear-induced diffusion of particles occurs because individual particles undergo random displacements from streamlines in a shear flow as they interact with and tumble over other particles [18]. The solute flux estimated based on the above mechanisms are quite different from each other, since the Brownian model predicts a decrease in flux with increasing particle size ($J_v \propto 1/{d_p}^{2/3}$) [17] while the shear-induced model predicts an increase in flux with increasing particle size ($J_v \propto {d_p}^{4/3}$) [18]. To include the particle size effect in the critical flux estimation, and using $d_p = 100$ nm as the reference point, for the transition from Brownian to shear-induced diffusion control [19], gives

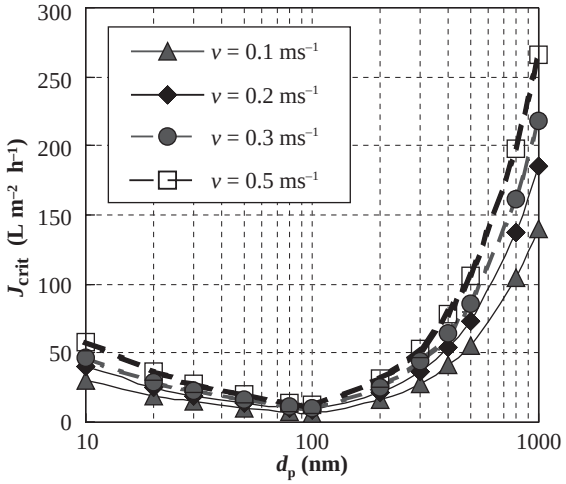

Fig. 2. J_{crit} as a function of d_p at different crossflow velocities.

$$\text{Brownian diffusion}: d_p \le 100 \text{ nm}, \frac{J_{crit,\,d_{p2}}}{J_{crit,\,d_{p1}}} = \left(\frac{d_{p1}}{d_{p2}}\right)^{2/3}, \tag{31}$$

$$\text{Shear-induced diffusion}: d_p > 100 \text{ nm}, \frac{J_{crit,\,d_{p2}}}{J_{crit,\,d_{p1}}} = \left(\frac{d_{p2}}{d_{p1}}\right)^{4/3}. \tag{32}$$

The critical flux is plotted as a function of particle size and crossflow velocities in Fig. 2.

Table 1
Input parameters for simulations

Fixed input parameters for all sections				
$W = 0.06$ m		$H = 1.4 \times 10^{-3}$ m	$\mu = 1.0 \times 10^{-3}$ Pa s	$R_m = 1.0 \times 10^{14}$ m^{-1}
$L = 0.31$ m		$\rho_p = 2410$ kgm^{-3}	$D = 1.5 \times 10^{-9}$ m^{2}s^{-1}	$R_{real} = 0.99$
Section	Variables	Input parameters		
4.1.	C_b, d_p, J_v or J_0	$d_p = 20$ nm	$C_{b,SiO_2} = 0.2$ kgm^{-3}	CP(0) = 1.2
4.2.1.	J_{crit}	$d_p = 20$ nm	$C_{b,SiO_2} = 0.2$ kgm^{-3}	$C_b = 2$ kgm^{-3}
		$v = 0.1$ ms^{-1}	J_v or $J_0 = 40$ L m^{-2} h^{-1}	
4.2.2.	v	$d_p = 20$ nm	$C_{b,SiO_2} = 0.2$ kgm^{-3}	
		$C_b = 2$ kgm^{-3}	J_v or $J_0 = 40$ L m^{-2} h^{-1}	
4.2.3.	J_v or J_0	$d_p = 20$ nm	$C_{b,SiO_2} = 0.2$ kgm^{-3}	
		$C_b = 2$ kg m^{-3}	$v = 0.1$ ms^{-1}	
4.2.4.	C_{b,SiO_2}	$d_p = 20$ nm	$C_b = 2$ kg m^{-3}	
		$v = 0.1$ ms^{-1}	J_v or $J_0 = 30$ L m^{-2} h^{-1}	
4.2.5.	C_b	$d_p = 20$ nm	$C_{b,SiO_2} = 0.2$ kgm^{-3}	
		$v = 0.1$ ms^{-1}	J_v or $J_0 = 30$ L m^{-2} h^{-1}	
4.2.6.	d_p	$v = 0.1$ ms^{-1}	$C_{b,SiO_2} = 0.2$ kgm^{-3}	
		$C_b = 2$ kg m^{-3}	J_v or $J_0 = 30$ L m^{-2} h^{-1}	

3. Methodology

It is relevant to compare the relative impact of the fouling resistance, R_f, and the CEOP effect (reduces the driving force) on the loss of performance in RO separation. The performance loss involves an increase in TMP ($\triangle$TMP = TMP(t) − TMP(0)) for constant flux operation, or a decrease in flux ($\triangle J_v = J_v(0) - J_v(t)$) for constant pressure operation. The procedures to estimate the value of TMP(t) or $J_v(t)$ based on the model presented in Section 2, are as follows:

(a) To estimate the TMP, TMP(t), for constant flux operation:

Input: W, L, H, μ, D, ρ_p, d_p, C_b, C_{b,SiO_2}, J_v, v, R_{real}, R_m, and t.

Step 1: Compute $k_m(0)$, CP(0), and TMP(0) from Eqs. (1), (4), (10), (18), and (19).
Step 2: Compute $m_f(t)$ from Eqs. (29)–(32).
Step 3: Estimate $\varepsilon(t)$ and compute $\alpha_f(t)$ from Eq. (26) and $\delta_c(t)$ from Eq. (28).
Step 4: Compute CP(t) from Eq. (16) and J_v.
Step 5: Compute $C_w(t)$ from Eqs. (2) and (9).
Step 6: Compute $\alpha_f(t)$ from Eq. (27).
Step 7: Solve for $\varepsilon(t)$ as such $\alpha_f(t)_{Step\ 3} - \alpha_f(t)_{Step\ 6} = 0$. Recalculate $\alpha_f(t)$, $\delta_c(t)$, CP(t), and $C_w(t)$ with the new value of $\varepsilon(t)$.
Step 8: Compute $R_f(t)$ from Eq. (25).
Step 9: Compute TMP(t) from Eq. (20).
Step 10: Calculate the contribution of CEOP and R_f from Eq. (21).

(b) To estimate the operating flux, $J_v(t)$, for constant pressure operation:

Input: W, L, H, μ, D, ρ_p, d_p, C_b, C_{b,SiO_2}, $J_v(0)$, v, R_{real}, R_m, and t.

Step 1: Compute $k_m(0)$, CP(0), and TMP from Eqs. (1), (4), (10), (19), and (22).
Step 2: Estimate $J_v(t)$ and compute $m_f(t)$ from Eqs. (29)–(32).
Step 3: Estimate $\varepsilon(t)$ and compute $\alpha_f(t)$ from Eq. (26) and $\delta_c(t)$ from Eq. (28).
Step 4: Compute CP(t) from Eq. (16) and $J_v(t)$ from Step 2.
Step 5: Compute $C_w(t)$ from Eqs. (2) and (9).
Step 6: Compute $\alpha_f(t)$ from Eq. (27).
Step 7: Compute $R_f(t)$ from Eq. (25).
Step 8: Compute $J_v(t)$ from Eq. (23).
Step 9: Solve for $\varepsilon(t)$ as such $\alpha_f(t)_{Step\ 3} - \alpha_f(t)_{Step\ 6} = 0$ and $J_v(t)_{Step\ 2} - J_v(t)_{Step\ 8} = 0$.
Recalculate $\alpha_f(t)$, $\delta_c(t)$, CP(t) and $C_w(t)$, $R_f(t)$, and $J_v(t)$ with the new value of $\varepsilon(t)$.
Step 10: Calculate the contribution of CEOP and R_f from Eq. (24).

The calculations are solved with Microsoft Excel. The input parameters for the simulations are summarized in Table 1.

4. Results and discussion

4.1. Simulations for fixed cake thicknesses

The first case considered assumes a membrane channel fouled by a cake layer with thickness of 10 and 50 μm. The initial CP (un-fouled) is assumed to be 1.2, which in practice the membrane manufacturers recommend a value of <1.2.

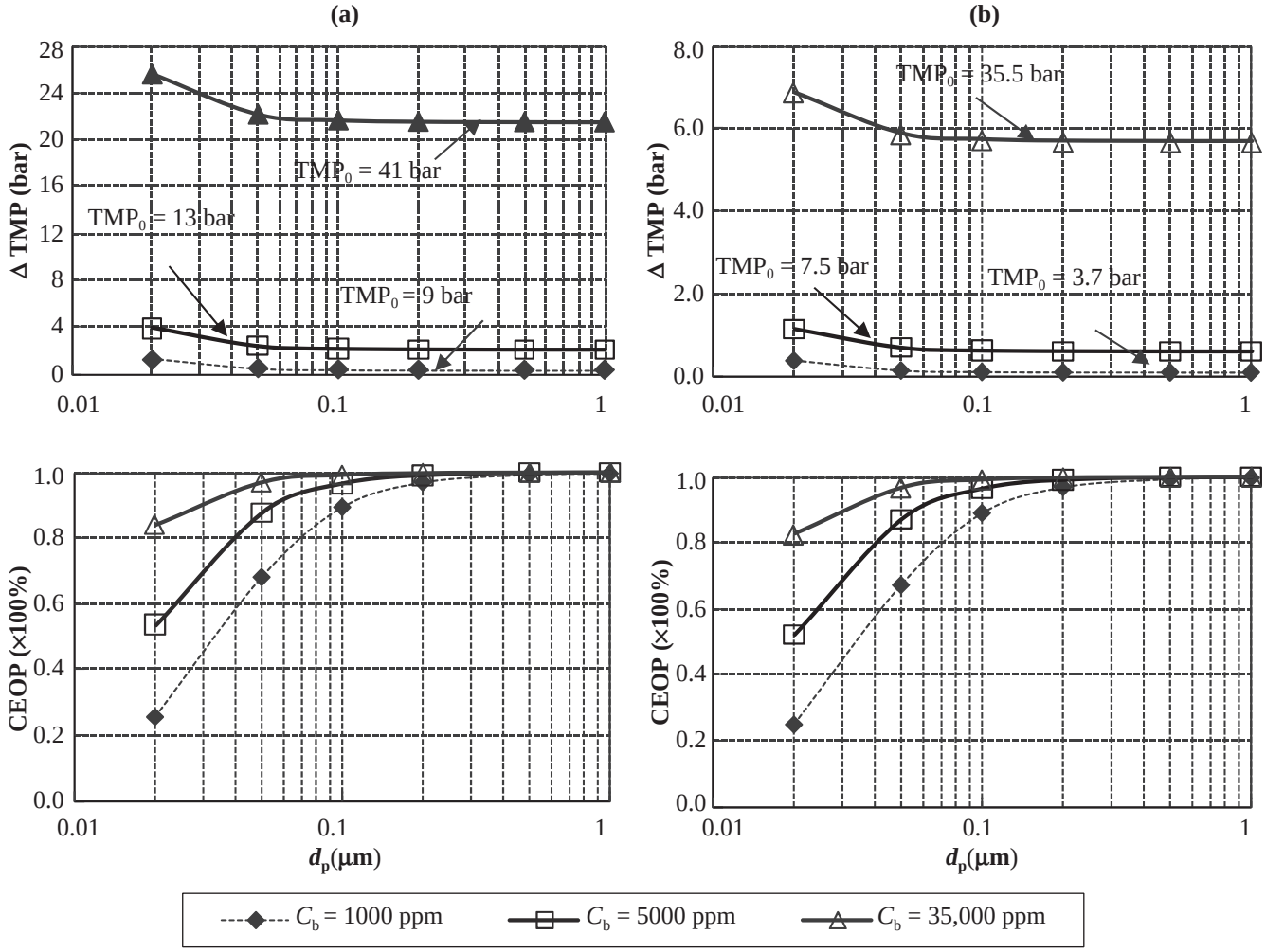

Fig. 3. △TMP and relative contribution of CEOP for fixed cake thickness of 10 μm at constant flux operation (a) $J_v = 30$ L m^{-2} h^{-1} and (b) $J_v = 10$ L m^{-2} h^{-1}.

4.1.1. Cake thickness of 10 μm

Fig. 3 presents the results of calculations for a cake thickness of 10 μm for constant fluxes of 30 and 10 L m^{-2} h^{-1}, respectively. The figures on the top show the responses as the required TMP increases, △TMP, or the reduction in flux, $\triangle J_v$. The figures on the bottom show the CEOP contributions. At constant flux operation, the contribution of CEOP upon △TMP is strongly affected by the particle size, d_p. For instance, when $d_p >$ 100 nm, more than 90% of the TMP rise is due to the CEOP effect regardless of the operating flux, J_v, or salt concentration, C_b. R_f does not play a significant role in the TMP increase. Whereas for $d_p < 100$ nm, △TMP increases exponentially with decrease in the particle size and the CEOP effect decreases. Also, the TMP increase due to the CEOP effect is influenced by C_b. For example, at $d_p = 20$ nm and $J_v = 30$ L m^{-2} h^{-1}, the contribution by CEOP upon △TMP is 25%, 55%, and 85% at C_b of 1000, 5000, and 35,000 ppm, respectively. However, the contribution by CEOP due to flux increase, e.g. increasing the J_v from 10 to 30 L m^{-2} h^{-1}, is less than 5% only for the same d_p and C_b.

The trends at constant pressure operation (as shown in Fig. 4 for $J_0 = 30$ and 10 L m^{-2} h^{-1}) have a similar pattern to those at constant flux operation. When a particle is greater than 100 nm, $\triangle J_v$ is solely due to CEOP. For d_p < 100 nm, a greater CEOP component is observed as particle size increases, as salt concentration increases and for the higher flux condition. But the % contribution of CEOP upon $\triangle J_v$ is less than in the constant flux operation upon △TMP. This observation is more obvious when operating at lower J_0. This is because the concentration polarization modulus, CP, is driven by flux, and as flux declines due to fouling in the constant pressure mode, then CP also drops. Hence, the contribution of R_f is more significant in this case.

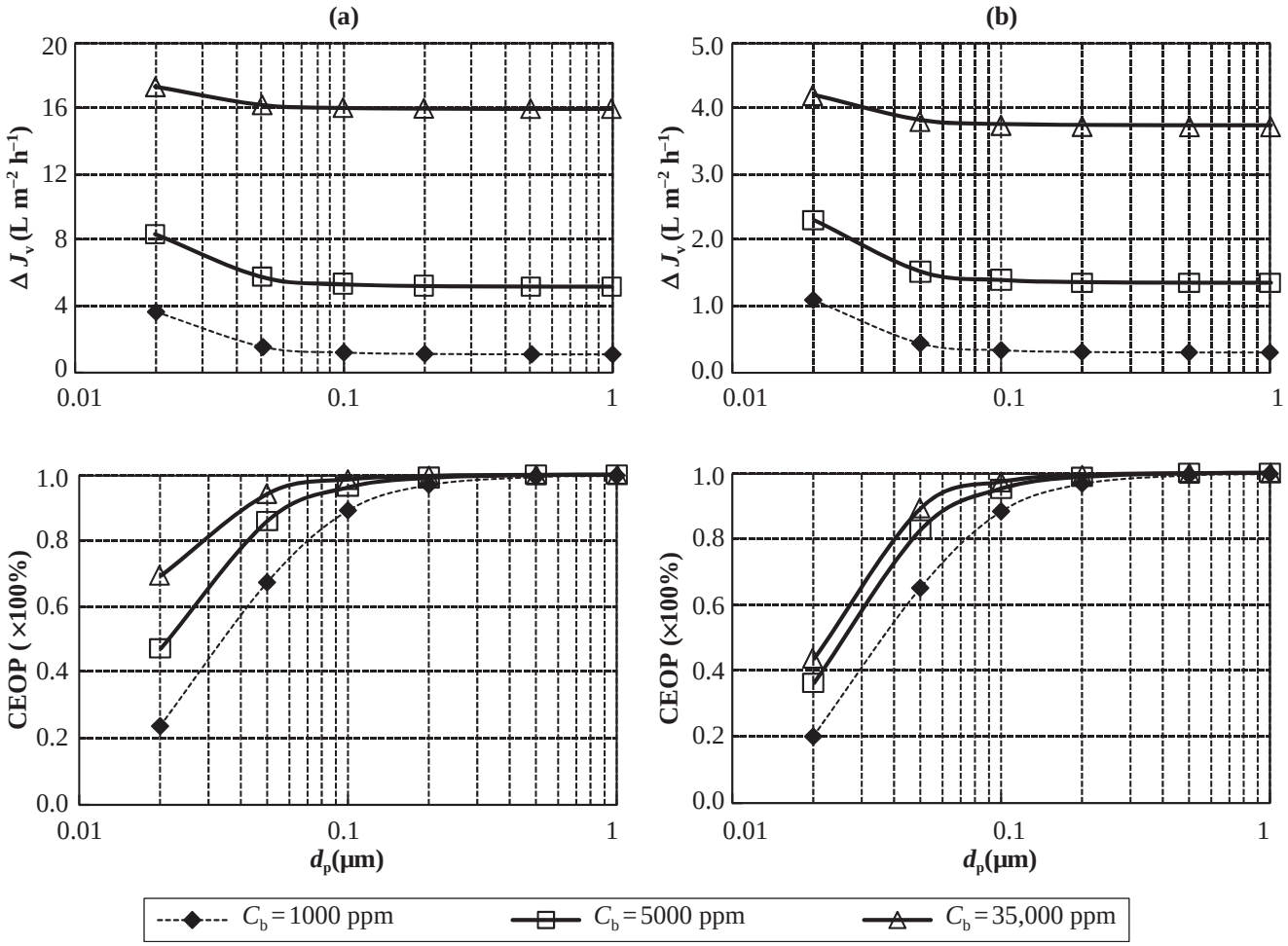

Fig. 4. $\triangle J_v$ and relative contribution of CEOP for fixed cake thickness of 10 μm at constant pressure operation (a) $J_0 = 30$ L m^{-2} h^{-1} and (b) $J_0 = 10$ L m^{-2} h^{-1}.

4.1.2. Cake thickness of 50 μm

As shown in Fig. 5(a) and (b), at constant flux operation of 30 and 10 L m^{-2} h^{-1}, respectively, a thicker cake layer leads to a greater contribution by CEOP upon the overall TMP increase when $d_p < 100$ nm. For example, the contribution by CEOP is 35%, as compared to only 25% at the cake thickness of 10 μm when $d_p = 20$ nm, $C_b = 1000$ ppm, and $J_v = 30$ L m^{-2} h^{-1}. Moreover, the CEOP effect also increases with increasing d_p, C_b, and J_v. Again, when the particle is greater than 100 nm, the contribution of R_f can be ignored.

Generally, in the constant pressure mode, trends are similar to those observed for the cake thickness of 10 μm (Fig. 5(c) and (d)). Further, only a minute change in the % contribution by CEOP upon $\triangle J_v$ is observed even though the cake is getting thicker, e.g. at $d_p = 20$ nm, $C_b = 1000$ nm, and $J_0 = 30$ L m^{-2} h^{-1}, the contribution by CEOP is ~25% at both cake thicknesses.

4.1.3. Discussion

Overall, for particles of 100 nm and larger the major fouling effect appears to be CEOP, rather than a fouling resistance. The CEOP effect is less for feed with a low salt content; in the extreme where there are no 'osmotic solutes' then there is no need to compensate for the osmotic effect. The above calculations have been based on cakes of colloidal silica particles. However, biofilms also provide an unstirred layer analogous to cakes. Biofilms develop from deposited bacteria that adhere and accumulate by growth on the membrane surface. The major fouling component of a biofilm is due to extracellular polymeric substances (EPS), which has a measured specific resistance of the order of 0.5×10^{16} m kg^{-1} [20], equivalent to a 20 nm sized fine colloid (assuming $\varepsilon \sim 0.3$). The deposited layers of EPS could also cause CEOP. As shown in our previous work [2], a model EPS, alginic acid, can

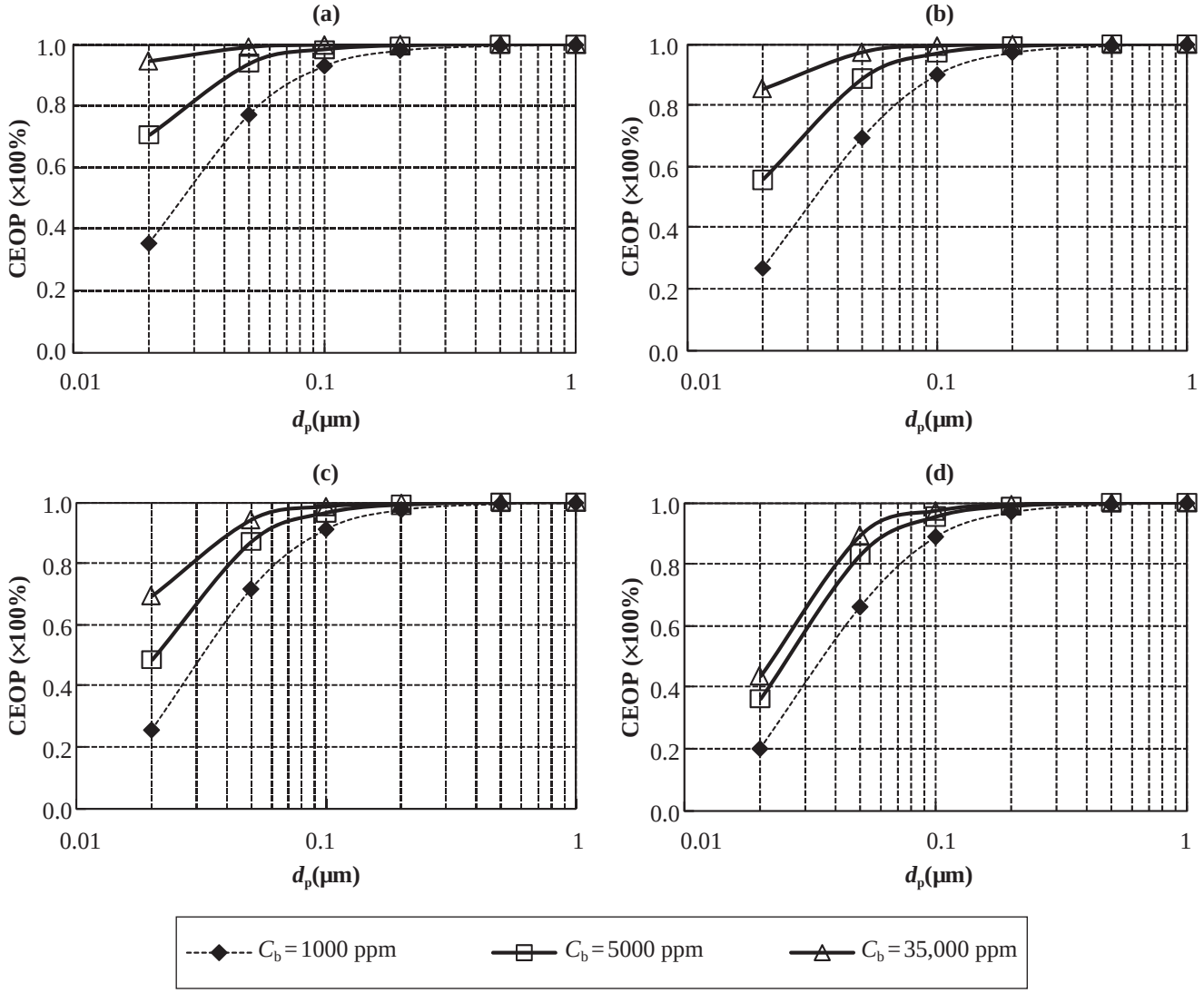

Fig. 5. Relative contribution of CEOP for fixed cake thickness of 50 μm at (a) $J_v = 30$ L m^{-2} h^{-1} (constant flux), (b) $J_v = 10$ L m^{-2} h^{-1} (constant flux), (c) $J_0 = 30$ L m^{-2} h^{-1} (constant pressure), and (d) $J_0 = 10$ L m^{-2} h^{-1} (constant pressure).

create a higher loss in the driving force due to the CEOP effect than the hydraulic resistance the flux is greater than 20 L m^{-2} h^{-1}.

4.2. Kinetics of TMP increase or flux drop and relative contributions of CEOP

The results presented in the previous section are based on fixed cake thickness. This section will look into the dynamics of the build-up of the cake and development of CEOP under the effect of critical flux, crossflow velocity, operating flux, particle concentration, salts concentration and particle size, and their impacts on the membrane performance.

4.2.1. Varying critical flux, J_{crit}

The first case to consider is the effect of higher critical flux on fouling. Critical flux, J_{crit}, due to particulate fouling can be improved by various methods such as coagulation forming bigger particles [21,22], and the use of electrical fields [23]. Undeniably, the use of such techniques will modify either the solution physical and chemical properties, or hydrodynamic conditions, but only the change in the critical flux value is considered here, and other parameters are assumed unchanged in the calculations. As shown in Fig. 6(a), at constant flux operation, as J_{crit} increases, $(J_v - J_{crit})$ decreases, resulting in a lower net deposition rate, i.e. the cake layer formed is thinner. This results in a slower build-up in

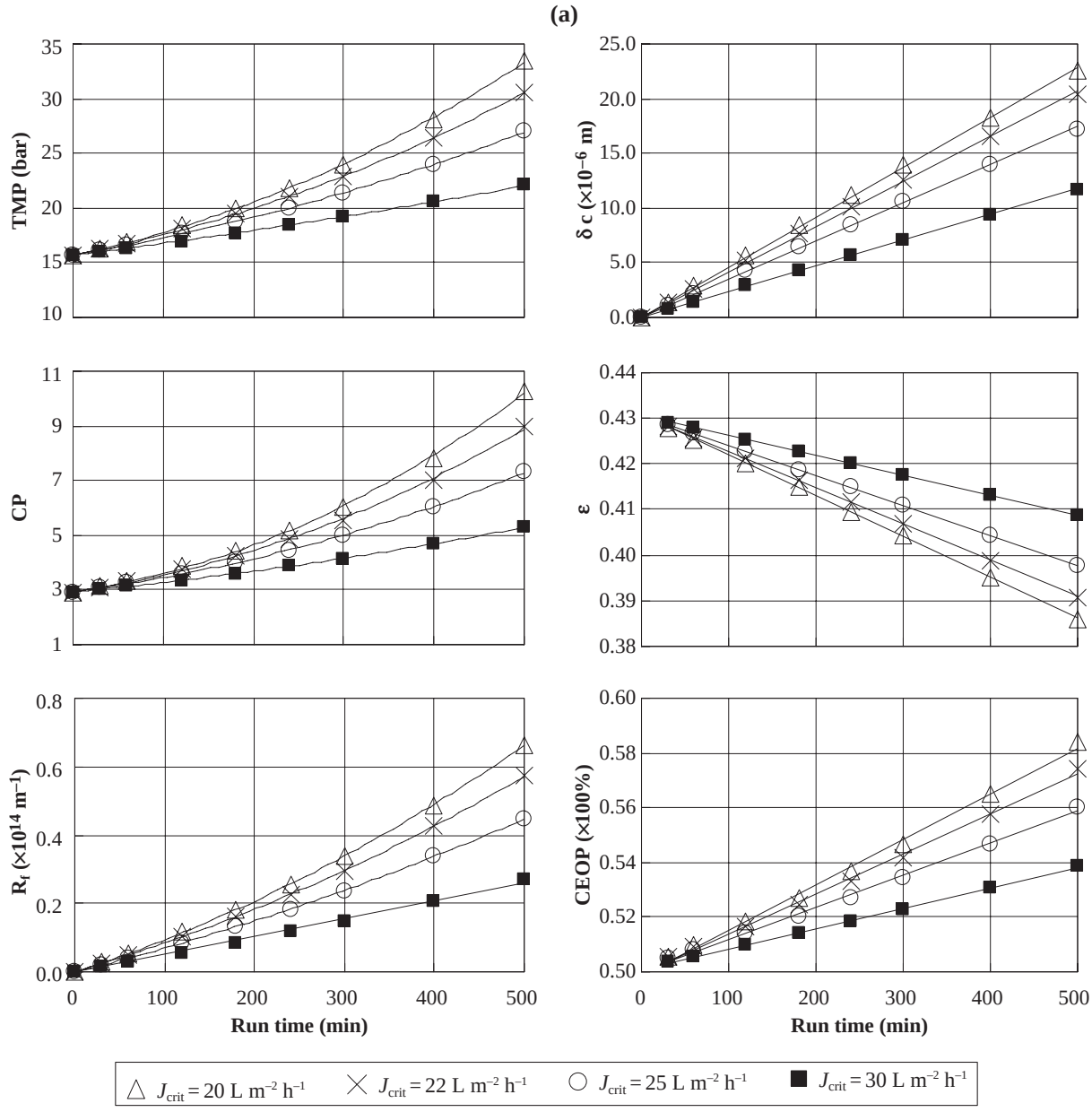

Fig. 6. *Continued*

the cake resistance, R_f, and CP level. In this example, a 50% increase in J_{crit}, from 20 to 30 L m^{-2} h^{-1}, reduces increase in $\triangle$TMP by $\sim$53%. In addition, the contribution of CEOP to $\triangle$TMP is the lowest at the highest J_{crit}. The CEOP effect increases over time and becomes the controlling fouling mechanism.

It should be noted that the fouling in terms of the cake build-up rate, $d\delta_c/dt$, is a steady rise but the effect, observed as $dTMP/dt$, tends to be accelerating due to the non-linear contribution of CP according to Eq. (17). This is more obvious at higher net flux than at lower net flux where the TMP and CP rise can be treated as near-linear (straight lines in the plot).

In the fixed pressure mode, δ_c increases rapidly initially then increases slowly, and eventually reaches an asymptotic value, unlike in the fixed flux mode where there is a continuous accumulation with time. As J_{crit} increases, the rate of flux drop also decreases due to less foulants deposited over time (Fig. 6(b)). Since the flux decline rate is at the minimum for the highest level of J_{crit}, in other words, the transient flux level is the highest, the contribution of CEOP is the highest. However, the CEOP effect remains relatively steady over time as fouling progresses, i.e. at J_{crit} = 30 L m^{-2} h^{-1}, less than 0.2% change in the CEOP contribution is observed after 500 min of operation.

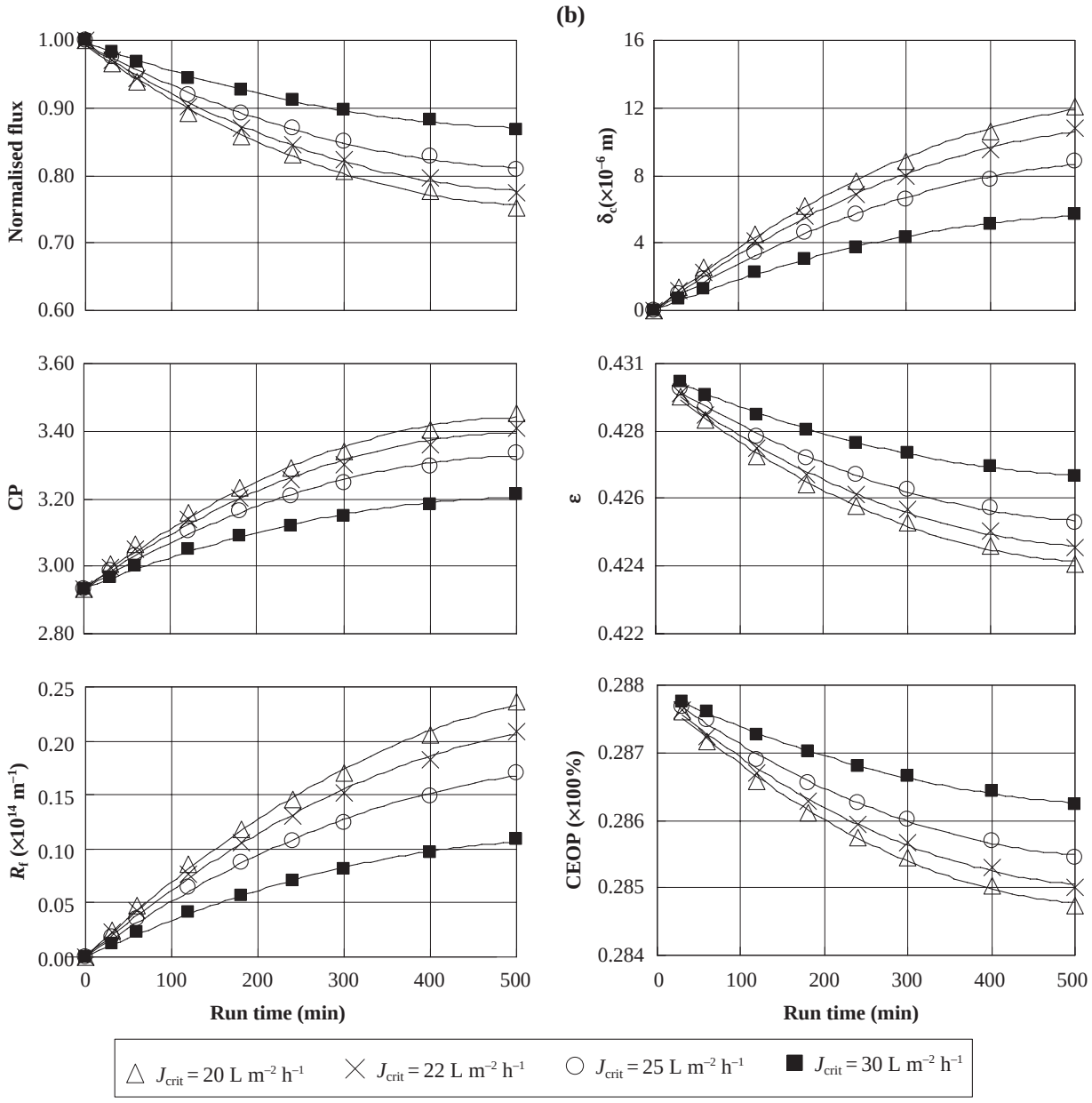

Fig. 6. (a) Varying J_{crit} at constant flux operation. (b) Varying J_{crit} at constant pressure operation.

Moreover, the contribution of CEOP in constant pressure mode ($\sim$28%) is notably less than in constant flux operation (>50%). This can be explained since J_v drops due to fouling in the fixed pressure operation, and, therefore, a lower J_v gives a lower CP value according to Eq. (17).

4.2.2. Varying crossflow velocity, v

Increasing the crossflow velocity results in an increase in the critical flux level due to higher back transport of particles induced by shear (see Eq. (30)). This can have significant impact on the rate of fouling. In constant flux operation, from Fig. 7(a), as v increases, the rate of change of TMP and CP is reduced drastically, from an exponential rise to a near-linear increase. For example, at $t = 500$ min, $\triangle$TMP is only $\sim$1.6 bar at $v = 0.50$ ms^{-1} as compared to at a lower crossflow of 0.10 ms^{-1} when the TMP is doubled, from 15.7 to 34.8 bar. At higher crossflow velocity, the CP value is lower, so the CEOP contribution is less than the R_f. Also, it should be noted that the improvement in membrane performance at higher crossflow velocity, is better than in the previous case, resulting in higher critical

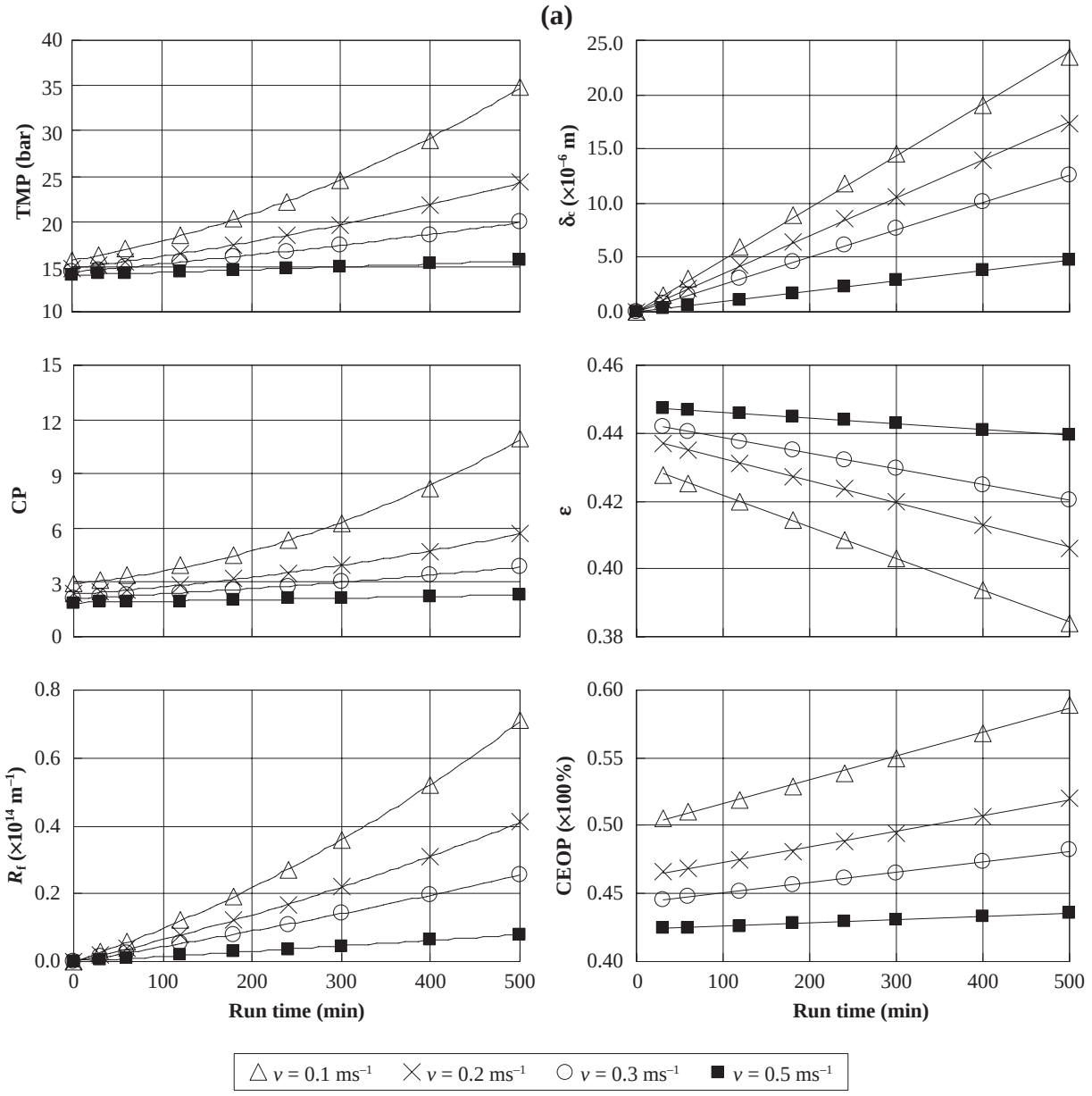

Fig. 7. *Continued*

flux. For example, in the previous simulation increasing the critical flux from 20 to 30 L m^{-2} h^{-1} at v = 0.10 ms^{-1}, reduces the △TMP from 17.7 to 6.5 bar at t = 500 min (refer to Fig. 6(a)). A similar improvement in J_{crit}, from 20 to 30 L m^{-2} h^{-1}, can also be achieved by increasing the crossflow velocity from 0.10 to 0.30 ms^{-1}, which also results in a further reduction in △TMP, down to 5.5 bar. This is because apart from improving J_{crit}, the CP level is also lowered at higher crossflow velocity since CP = exp(J_v/k_m), whereby k_m is a function of crossflow velocity. Therefore, the relative CEOP effect appears to be lower, ~45% as compared to the previous case where CEOP is >50%. This suggests that other benefits, rather than an improvement in the critical flux level alone, should be considered when selecting an appropriate technique/treatment to reduce fouling.

In general, in the constant pressure mode, the rate of flux drop, CP and R_f build-up rate decreases with increasing crossflow velocity as shown in Fig. 7(b). Since the transient value of J_v is higher at high crossflow velocity of 0.50 ms^{-1} due to less fouling as compared to a low crossflow of 0.10 ms^{-1}, the contribution of CEOP is also the highest. Again, as in the first case, the CEOP

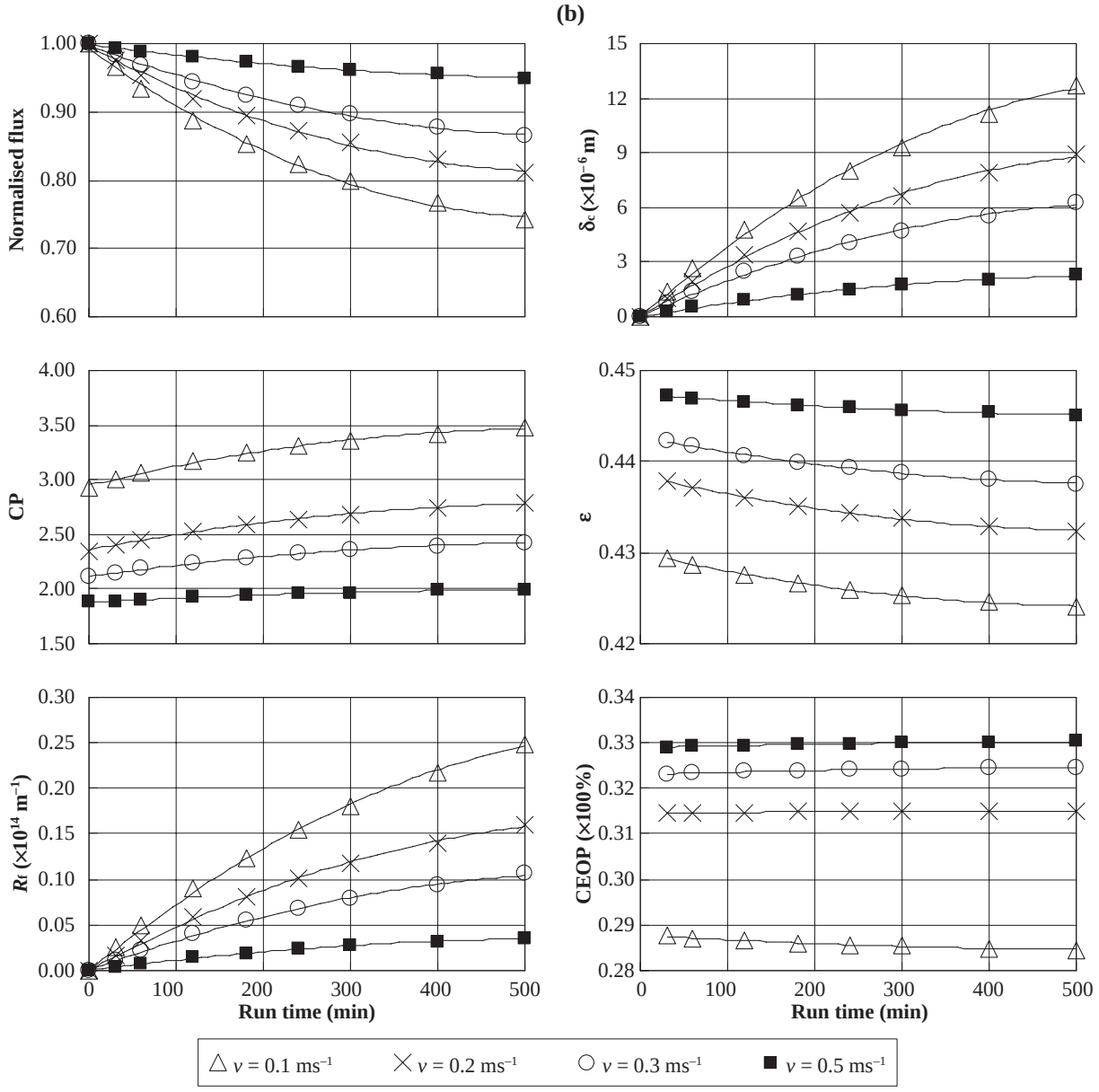

Fig. 7. (a) Varying v at constant flux operation. (b) Varying v at constant pressure operation.

effect in the fixed pressure operation is much lower than that in the constant flux mode.

It should also be noted that the fractional deposition constant, Φ, in Eq. (29) may be less than 1.0 for high crossflow velocities [9]. The effect of this is to slow down the rate of deposition. For example, if Φ is 0.5, the simulated rates of change are halved, and so on.

4.2.3. Varying operating flux, J_v

In constant flux operation, increasing J_v gives a larger net flux, $(J_v - J_{crit})$, when J_{crit} is constant. This results in an increase in the TMP rise and CEOP effects due to higher deposition rate as depicted in Fig. 8(a). It should be highlighted that increasing the J_v only yields a linear increase in the cake accumulation since $m_f \propto (J_v - J_{crit})$. R_f increases near-linearly as well since $R_f \propto m_f$, but there is a slight deviation from linearity due to the effect of NaCl concentration on the specific cake resistance, α_f, according to Eq. (27). In contrast, the consequence of increasing J_v is an exponential increase in the CP level since $CP = \exp(J_v/k_m)$. Thus, there is a tremendous increase in the CEOP effect, from 50% to 60 %, in 500 min when operating at a high J_v of 40 L m^{-2} h^{-1}.

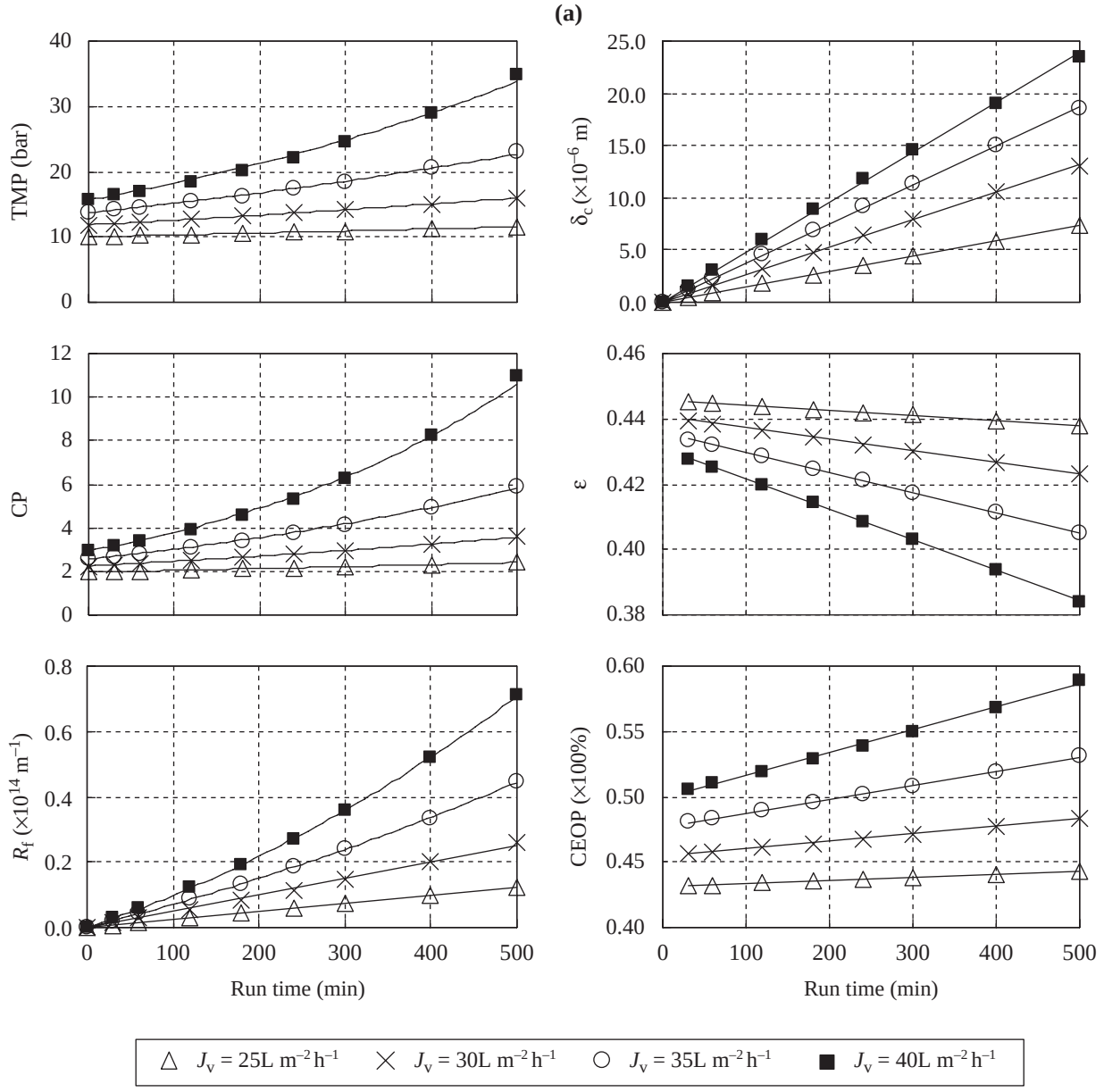

Fig. 8. *Continued*

Similarly, this principle applies when the net flux, $(J_v - J_{crit})$, is identical but with different combinations of J_v and J_{crit}. For example, when $J_v = 30$ L m^{-2} h^{-1}, $J_{crit} = 20$ L m^{-2} h^{-1} (Fig. 8(a)) and $J_v = 40$ L m^{-2} h^{-1}, $J_{crit} = 30$ L m^{-2} h^{-1} (Fig. 6(a)), where both give an equal net flux of 10 L m^{-2} h^{-1}. So the $d\delta_c/dt$ is same, ~13 μm in 500 min. However, there is an increase of 60% and 81% in the CP value in the first and second situation, respectively. This is simply due to higher J_v in the latter situation. This suggests that even if the critical flux is raised, it does not warrant the system to be operated at a higher flux level. It should be reminded that this outcome is only valid when the CEOP effect occurs, as R_f alone only produces a near-equal increase in TMP in both cases. Therefore, without taking into account the effect of CEOP, the intensity of fouling would be underestimated.

Similarly, operating at a higher initial flux, J_0, results in a greater flux decline rate, and thicker cake (Fig. 8(b)), although the $J_v(t)$ value is still higher at higher J_0 as compared to lower J_0, e.g. at $t = 500$ min, $J_v(t)$ is 22.5 and 30 L m^{-2} h^{-1} seen as a drop of 10% and 25% in the flux for J_0 of 25 and 40 L m^{-2} h^{-1}, respectively. Hence, the relative CEOP effect is higher for high J_0.

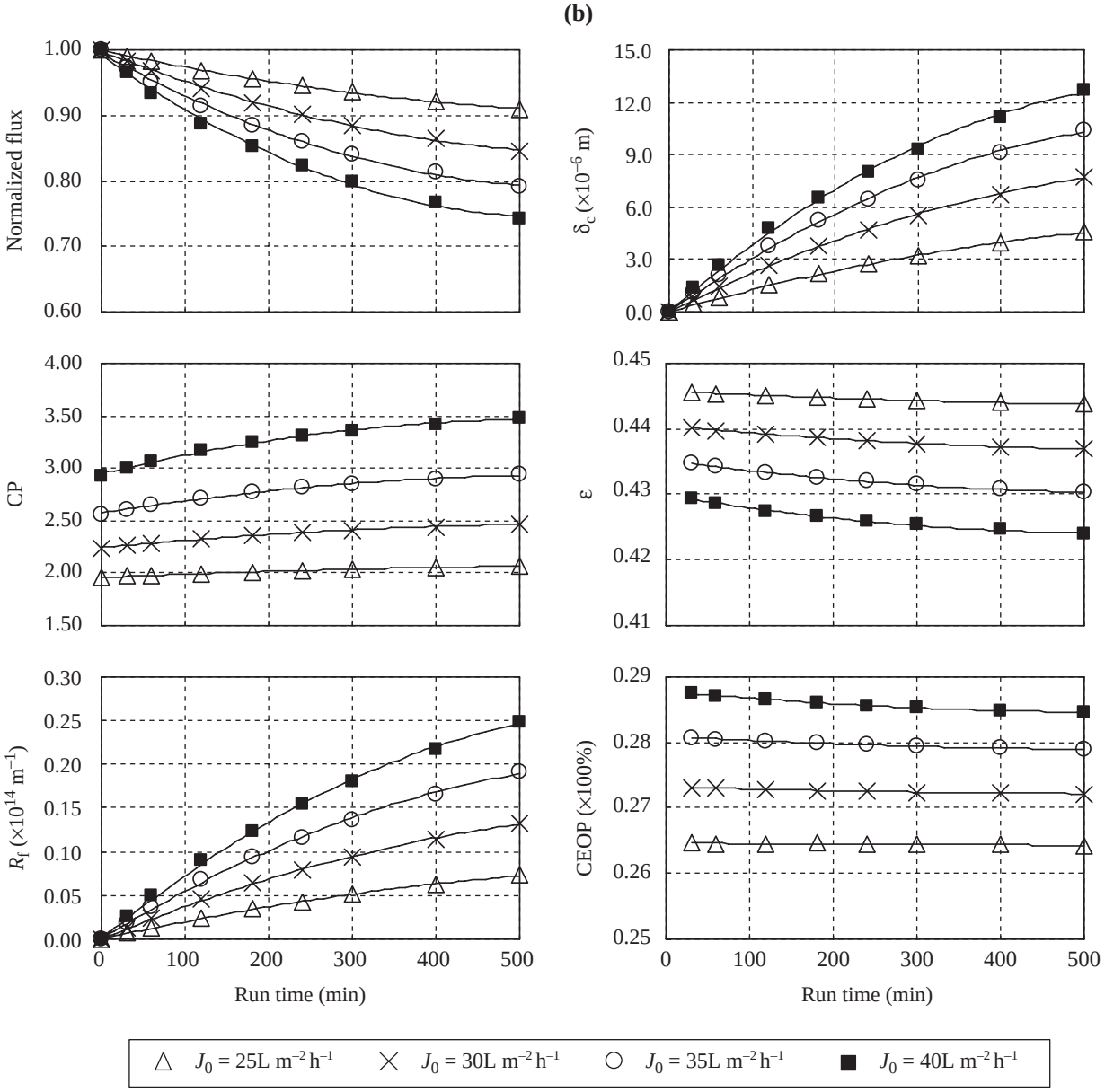

Fig. 8. (a) Varying J_v at constant flux operation. (b) Varying J_0 at constant pressure operation.

4.2.4. Varying particle concentration,C_{b,SiO_2}

The particle concentration in the feed solution can be controlled and reduced by microfiltration or ultrafiltration pretreatment processes. As expected, reducing C_{b,SiO_2} will slow down the cake formation rate and TMP increase rate as shown in Fig. 9(a). Similar to the situation presented above, R_f increases near-linearly while CP increases exponentially with increasing C_{b,SiO_2}. This can be reasoned with a linear increase in m_f and hence δ_c, but an exponential trend in CP value with δ_c.

Likewise, operation at fixed pressure, as C_{b,SiO_2} increases, $\triangle J_v$, δ_c, and R_f also increase as shown in Fig. 9(b). The contribution by the CEOP upon $\triangle J_v$ is lower at higher particle concentration, but the rate of change is less than 1% in 500 min. Again, the contribution by R_f in $\triangle J_v$ is dominant.

4.2.5. Varying salt concentration, C_b

Fig. 10(a) presents the membrane performance data at various salt concentrations in constant flux operation. Theoretically, according to Eq. (29), the rate of accumulation of deposits at various salt concentrations is identical as m_f is only a function of C_{b,SiO_2}, J_v, and J_{crit}.

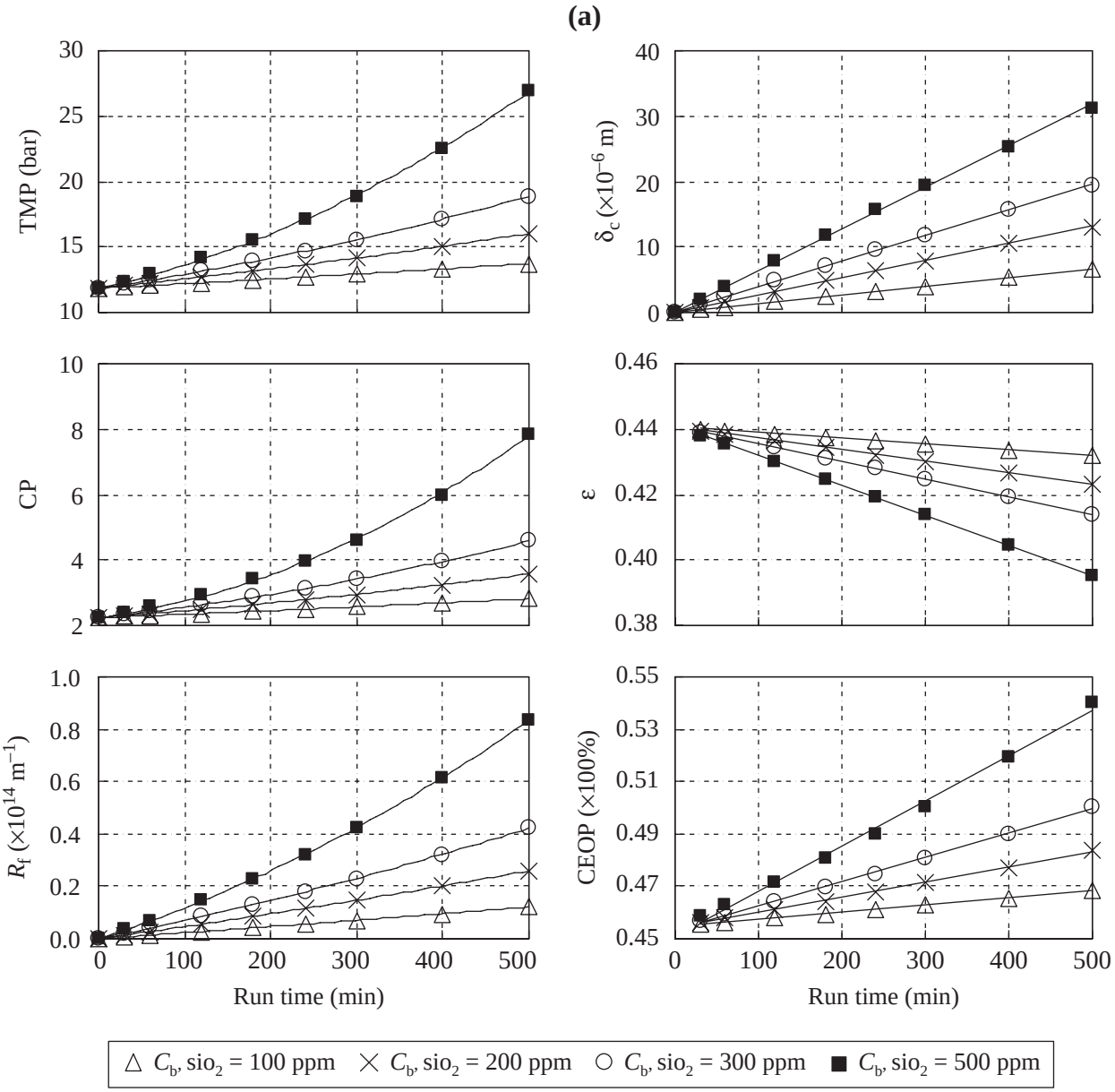

Fig. 9. *Continued*

The m_f vs. time plot is not shown here but the plot of cake thickness vs. time is presented instead. As seen, the thickness of cake decreases with increasing C_b (but the difference is not large) due to lower porosity, ε, at higher ionic strength thus forming a more compact cake layer (this is a consequence of Eqs. (26) and (27)); at such a low porosity, the specific cake resistance is high and so is R_f.

Since CP is also a function of ε (δ_c plays a less significant role here as the difference is small when C_b is increased), CP increases with increasing C_b and this ends up with a huge increase in the CEOP effect. The contribution of CEOP increases substantially from ~30% at 1000 ppm NaCl to ~90% at 35,000 ppm NaCl. This results in an exponential increase in △TMP at high ionic strength solution equivalent to seawater.

On the other hand, for constant pressure operation, increasing C_b results in a greater drop in flux as shown in Fig. 10(b). As expected, δ_c decreases with increasing C_b due to lower ε. R_f is still relatively high since α_f is high. However, unlike in the fixed flux situation, the CP decreases as C_b increases since there is a greater flux drop due to lower cake porosity and not due to thicker cake formation. Hence, the contribution by R_f is

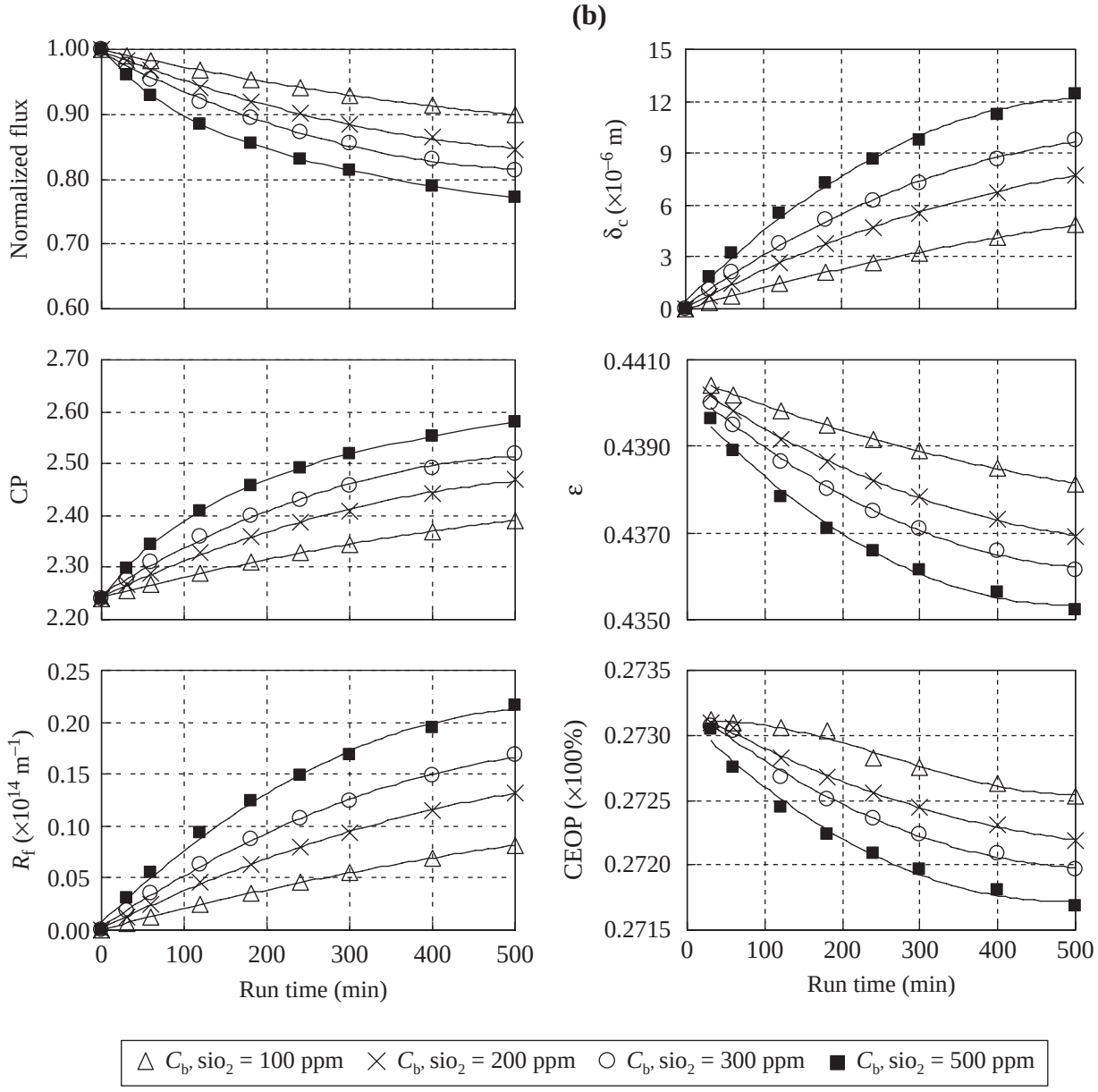

Fig. 9. (a) Varying C_{b,SiO_2} at constant flux operation. (b) Varying C_{b,SiO_2} at constant pressure operation.

dominant. These results agree with a recent study on colloidal silica fouling at different ionic strengths where more particle deposition was found at 10^{-2} M than at 10^{-1} M, but the latter has a larger hydraulic resistance because of the smaller effective porosity [24].

4.2.6. Varying particle size, d_P

4.2.6.1. Brownian diffusion

Fig. 11(a) shows the effect of particle size upon membrane performance at constant flux operation. For Brownian diffusion, increasing the particle size (up to 100 nm) decreases the J_{crit}. As a result, the net flux of foulant is higher and thus δ_c is higher with increasing d_P. This gives a greater development of CP. However, increasing the particle size greatly reduces the R_f since $\alpha_f \propto 1/d_P^2$. Therefore, the contribution of CEOP increases dramatically from ~45% to over 90% when d_P increases from 20 to 100 nm.

Similarly, at constant pressure, as d_P increases, the flux decline rate increases due to more deposition, which gives a higher CP level as shown in Fig. 11(b). Again, the CEOP effect becomes evident as R_f contribution is fading when d_P approaches 100 nm. When the particle is small, e.g. at 20 nm, the R_f is the main fouling mechanism and the effect is

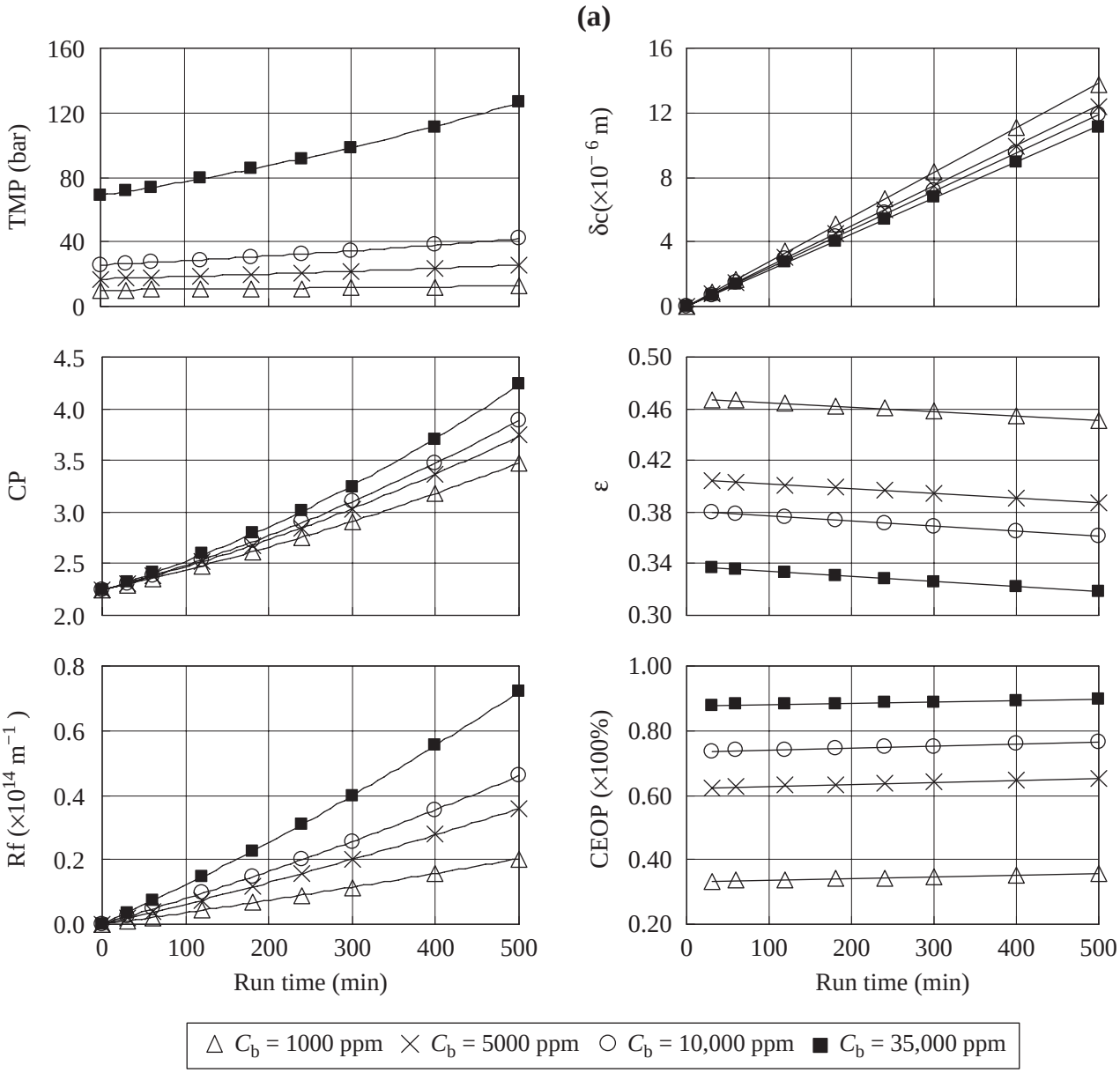

Fig. 10. *Continued*

more significant (~75%) than in the constant flux operation (~55%).

4.2.6.2. Shear-induced diffusion

The shear-induced diffusion mechanism is applicable to sub-micron sized particles with d_p > 100 nm. As opposed to Brownian diffusion, increasing the size for particles in the shear-induced diffusion region results in an increase in J_{crit} since $J_{crit} \propto {d_p}^{4/3}$. Hence, for both fixed flux (Fig. 11(c)) and fixed pressure operation (Fig. 11(d)), bigger particles give a lower rate of change of TMP in the former or less $\triangle J_v$ in the latter due to less deposition, lower CP, and R_f. The contribution by CEOP in both cases is greater than 90% for all the particle sizes.

The above results are supported by various studies of colloidal silica fouling in RO at fixed pressure using 300 nm-sized particles where the effect of trans-cake pressure ($\triangle P_c = J_v \mu R_f$) was less than 2% of the overall loss in the membrane performance [1,4,25].

5. Concluding remarks

A simple model has been developed to predict the membrane performance under the effect of critical flux

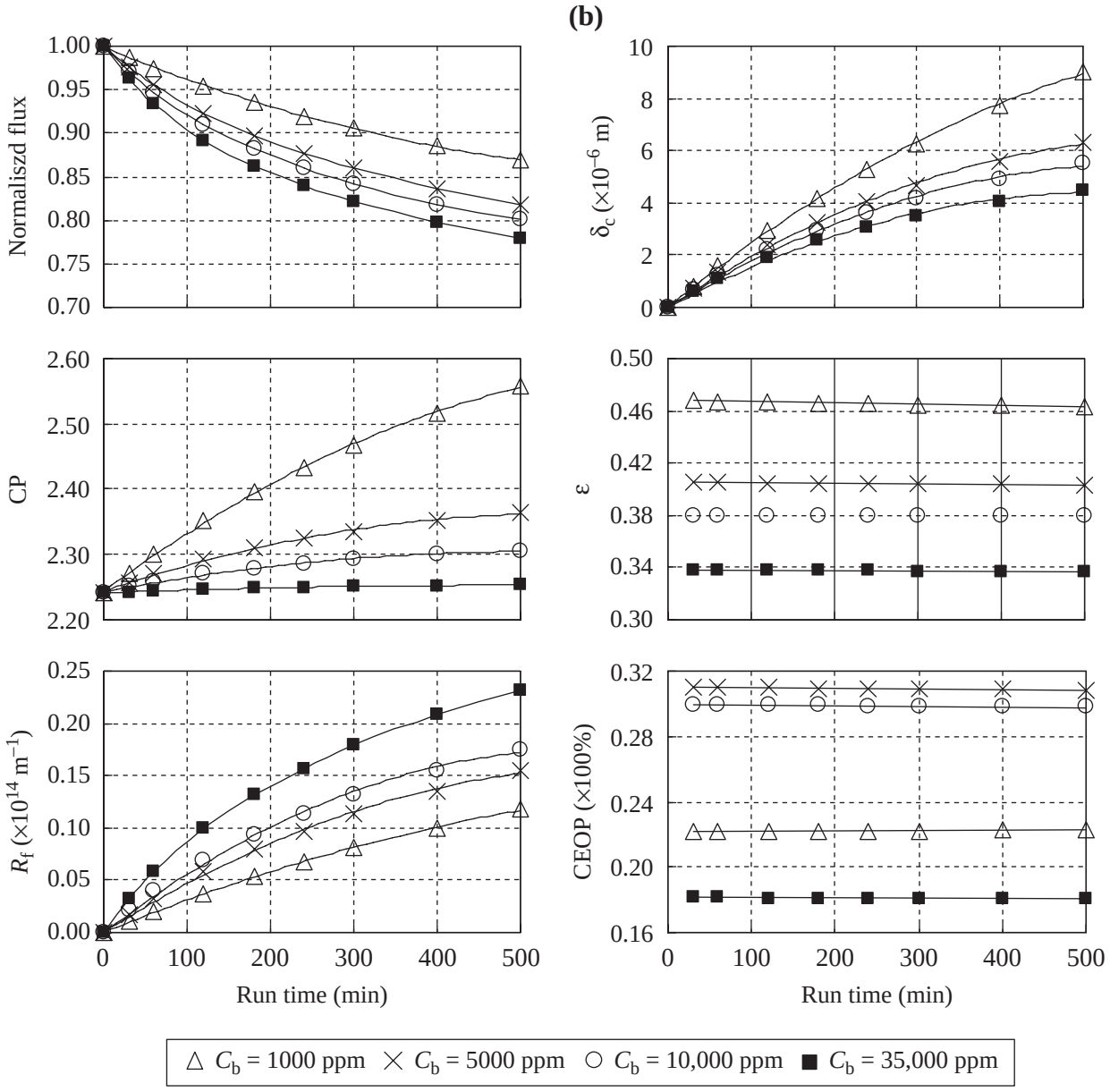

Fig. 10. (a) Varying C_b at constant flux operation. (b) Varying C_b at constant pressure operation.

(J_{crit}) and CEOP. In summary, for conventional constant flux operation the fouling in terms of rate of deposition, dm_f/dt, is a steady rise but the effect, observed as $dTMP/dt$, tends to be accelerating due to the non-linear contribution of CEOP. This happens at high net flux, low crossflow velocity, high particle loading, and high salt content. Also, it is found that the fouling mechanism is greatly controlled by the particle size. When d_p > 100 nm, regardless of the operating flux, crossflow velocity, critical flux, salt concentration, and particle concentration, the loss in membrane performance is predominantly due to the CEOP effect. When d_p is significantly less than 100 nm, other factors then play a part in the overall loss in performance. In constant flux operation, it is found that the transition from R_f controlled to CEOP controlled occurs when J_v, C_b, and C_{b,SiO_2} is high as well as when v and J_{crit} is low. It is also evident that the CEOP effect is greater at fixed flux operation than at fixed pressure operation simply due to the decline in flux, hence CP, in the latter situation.

Glossary

Symbol	Description (units)
C	Concentration of solute (ppm or kgm^{-3})

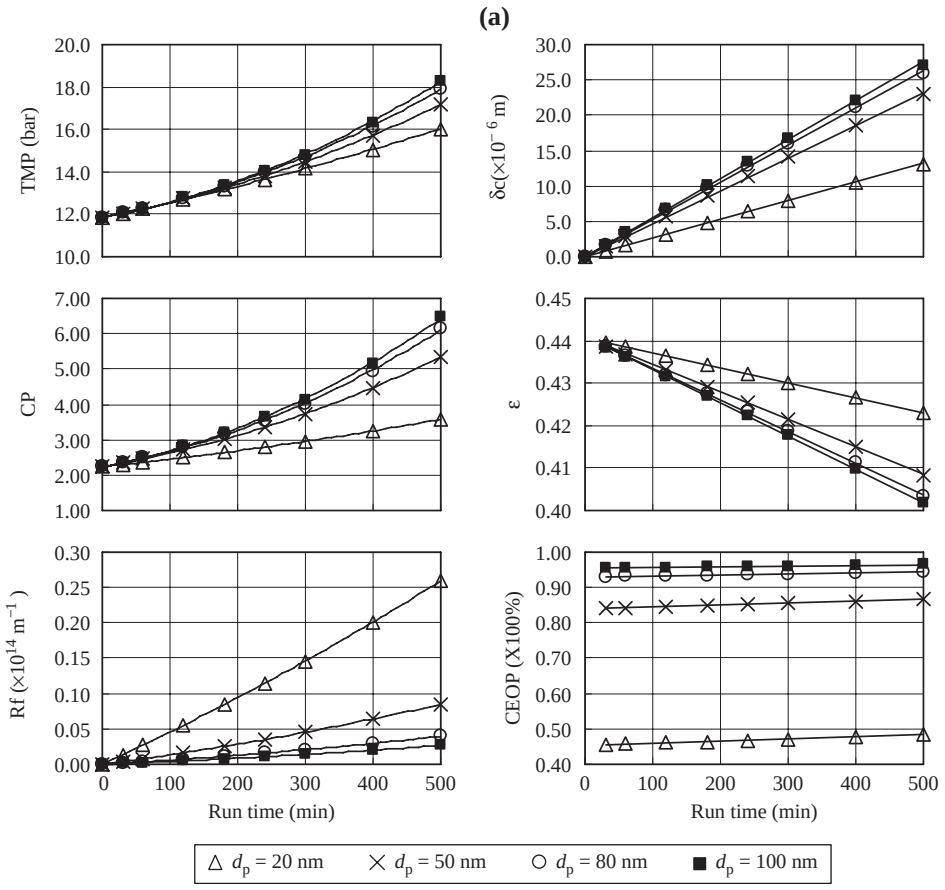
(a)
TMP (bar)
δc(×10⁻⁶ m)
CP
ε
Rf (×10¹⁴ m⁻¹)
CEOP (X100%)
Run time (min)
Run time (min)
△ d_p = 20 nm
× d_p = 50 nm
○ d_p = 80 nm
■ d_p = 100 nm

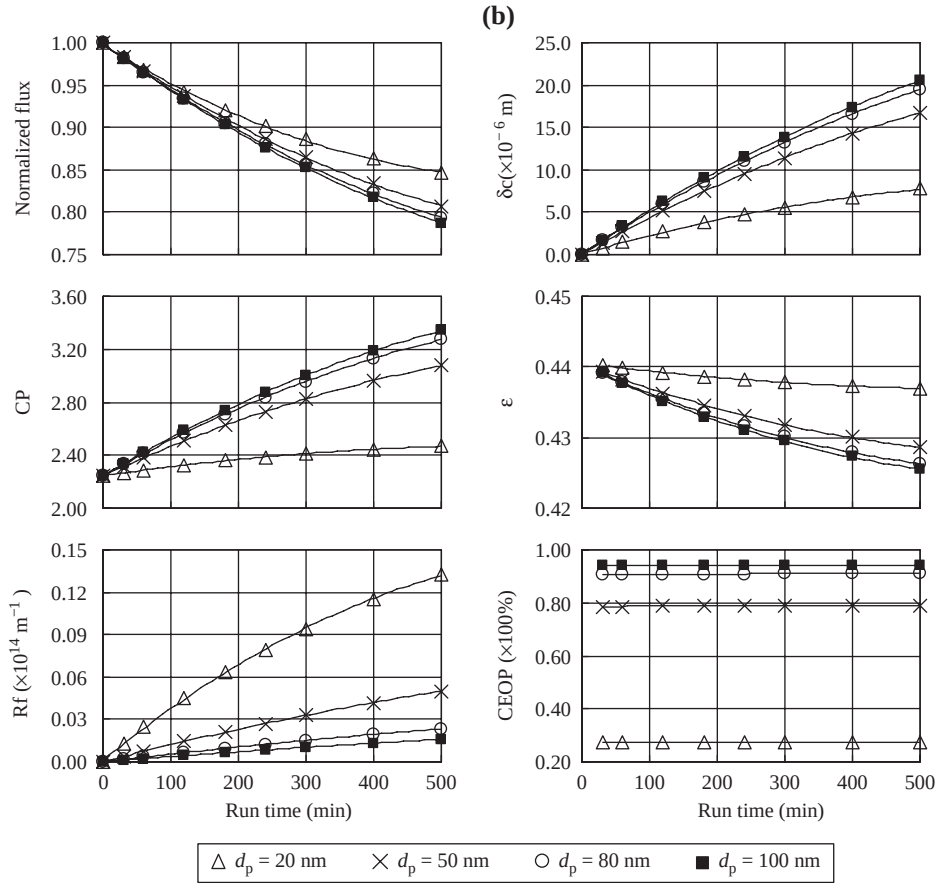
(b)
Normalized flux
δc(×10⁻⁶ m)
CP
ε
Rf (×10¹⁴ m⁻¹)
CEOP (×100%)
Run time (min)
Run time (min)
△ d_p = 20 nm
× d_p = 50 nm
○ d_p = 80 nm
■ d_p = 100 nm

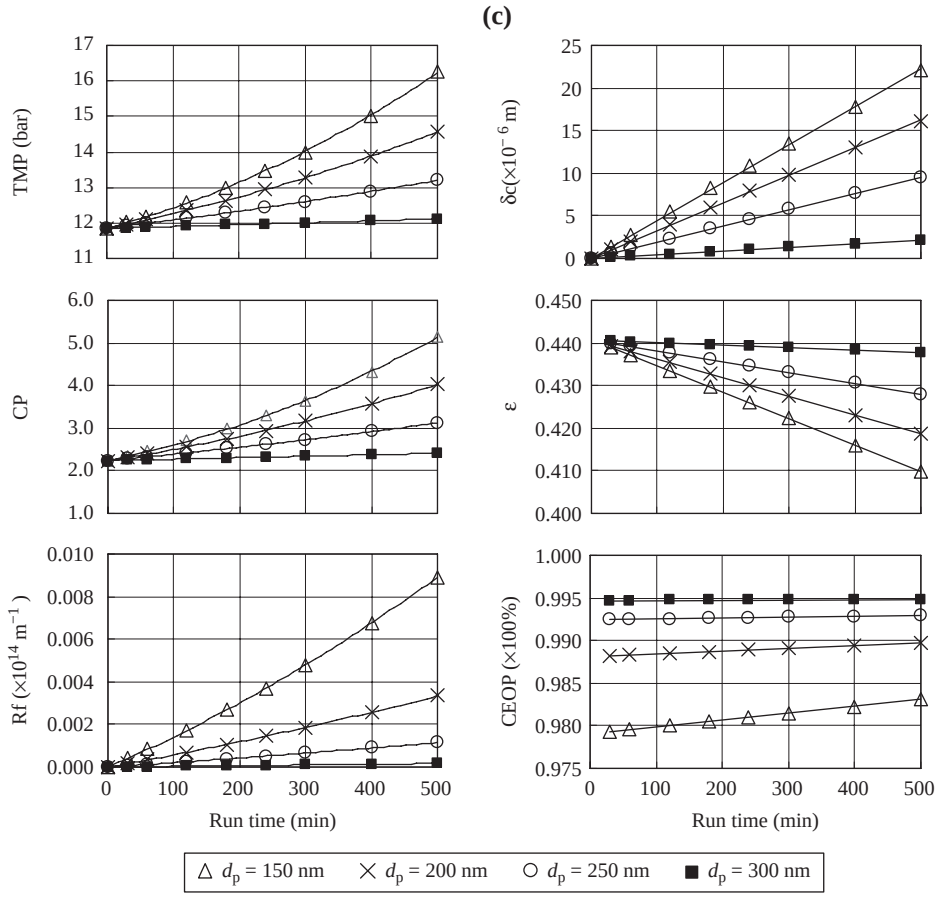

Fig. 11. *Continued*

C_b	Concentration of solute in bulk solution (ppm or kgm^{-3})	k_c	Mass transfer coefficient in cake layer (ms^{-1})
C_{b,SiO_2}	Concentration of silica colloids in bulk solution (ppm or kgm^{-3})	k_{eff}	Effective mass transfer coefficient (ms^{-1})
C_c	Concentration of solute at cake layer surface (ppm or kgm^{-3})	k_m	Mass transfer coefficient (ms^{-1})
C_p	Concentration of solute in permeate solution (ppm or kgm^{-3})	k_p	Mass transfer coefficient in polarized layer (ms^{-1})
C_w	Concentration of solute at membrane surface (ppm or kgm^{-3})	L	Membrane channel length (m)
CP	Concentration polarization modulus (dimensionless)	m_f	Mass of deposit per unit membrane area (kgm^{-2})
D	Diffusion coefficient of solute in bulk solution (m^2s^{-1})	Q	Volumetric crossflow rate (L min^{-1} or m^3s^{-1})
D_c	Diffusion coefficient of solute in cake layer (m^2s^{-1})	R_f	Fouling layer or cake resistance (m^{-1})
d_p	Diameter of particle (m)	R_m	Membrane resistance (m^{-1})
H	Membrane channel height (m)	R_{obs}	Observed retention (dimensionless)
J_{crit}	Critical flux (L m^{-2} h^{-1} or $m^3m^{-2}s^{-1}$)	R_{real}	Real retention (dimensionless)
J_v	Permeate flux (L m^{-2} h^{-1} or $m^3m^{-2}s^{-1}$)	T	Time (h or min or s)
$\triangle J_v$	Permeate flux drop (L m^{-2} h^{-1} or $m^3m^{-2}s^{-1}$)	TMP	Transmembrane pressure (Pa or bar)
		$\triangle$TMP	Transmembrane pressure increase (Pa or bar)
		v	Crossflow velocity (ms^{-1})
		W	Membrane channel width (m)

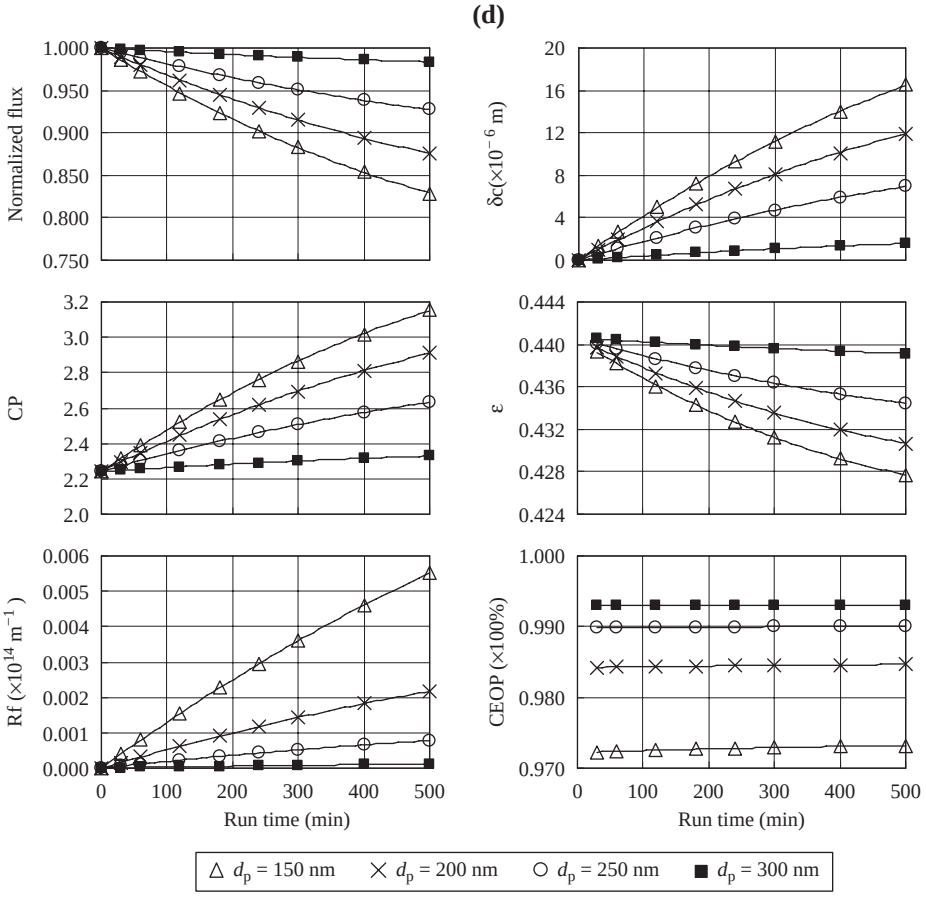

Fig. 11. (a) Varying d_P for Brownian diffusion at constant flux operation. (b) Varying d_P for Brownian diffusion at constant pressure operation. (c) Varying d_P for shear-induced diffusion at constant flux operation. (d) Varying d_P for shear-induced diffusion at constant pressure operation.

Greek letters

δ_P	Thickness of polarized layer (m)
δ_c	Thickness of cake layer (m)
α_f	Specific cake resistance (m kg^{-1})
μ	Viscosity of solution (Pa s)
ρ_P	Density of particle (kgm^{-3})
Φ	Fractional deposition constant (dimensionless)
ε	Cake porosity (dimensionless)
$\triangle\Pi_b$	Osmotic pressure difference between feed and permeate solution (Pa or bar)
$\triangle\Pi_w$	Osmotic pressure difference between membrane wall and permeate solution (Pa or bar)

Acknowledgements

The authors acknowledge financial assistance from A*STAR (Agency for Science, Technology and Research, Singapore) through support for the Temasek Professor Programme in Membrane Technology for Sustainable Water, and EWI (Environment & Water Industry Development Council, Singapore) for support for the Singapore Membrane Technology Centre. The authors also thank Prof. Wang Rong from Nanyang Technological University for her assistance in the modeling work.

References

[1] E.M.V. Hoek and M. Elimelech, Cake enhanced concentration polarization: a new fouling mechanism for salt-rejecting membranes, Environ. Sci. Technol., 37 (2003) 5581-5588.
[2] T.H. Chong, F.S. Wong and A.G. Fane, Enhanced concentration polarization by unstirred fouling layers in reverse osmosis: detection by sodium chloride tracer response technique, J. Membr. Sci., 287 (2007) 198-210.
[3] G. Singh and L. Song, Cake compressibility of silica colloids in membrane filtration processes, Ind. Eng. Chem. Res., 45 (2006) 7633-7638.
[4] E.M.V. Hoek, A.S. Kim and M. Elimelech, Influence of crossflow membrane filter geometry and shear rate on colloidal fouling in reverse osmosis and nanofiltration separations, Environ. Eng. Sci., 19 (2002) 357-372.
[5] B.P. Boudreau, The diffusive tortuosity of fine-grained unlithified sediments, Geochim. Cosmochim. Acta, 60 (1996) 3139-3142.

[6] C.F. Pan, Activity and osmotic coefficients in dilute aqueous solutions of uni-univalent electrolytes at 25°C, J. Chem. Eng. Data, 26 (1981) 183.
[7] P.C. Carman, Fluid flow through granular beds, Chem. Eng. Res. Des., 15 (1937) 150-166.
[8] R.M. McDonogh, C.J.D. Fell and A.G. Fane, Surface charge and permeability in the ultrafiltration of non-flocculating colloids, J. Membr. Sci., 21 (1984) 285-294.
[9] T.H. Chong, F.S. Wong and A.G. Fane, Implications of critical flux and cake enhanced osmotic pressure (CEOP) on colloidal fouling in reverse osmosis: experimental observations, J. Membr. Sci., 314 (2008) 101-111.
[10] J. Schwinge, P. Neal, D.E. Wiley and A.G. Fane, Estimation of foulant deposition across the leaf of a spiral wound module, Desalination, 146 (2002) 203-208.
[11] H. Li, A.G. Fane, H.G.L. Coster and S. Vigneswaran, Direct observation of particle deposition on the membrane surface during crossflow microfiltration, J. Membr. Sci., 149 (1998) 83-97.
[12] H. Li, A.G. Fane, H.G.L. Coster and S. Vigneswaran, Observation of deposition and removal behaviour of submicron bacteria on the membrane surface during crossflow microfiltration, J. Membr. Sci., 217 (2003) 29-41.
[13] P. Bacchin, P. Aimar and R.W. Field, Critical and sustainable fluxes: theory, experiments and applications, J Membr. Sci., 281 (2006) 42-69.
[14] G. Belfort, R.H. Davis and A.L. Zydney, The behaviour of suspensions and macromolecular solutions in crossflow microfiltration, J. Membr. Sci., 96 (1994) 1-58.
[15] W.R. Bowen and F. Jenner, Theoretical description of membrane filtration of colloids and fine particles: assessment and review, Adv. Colloid Interface Sci., 56 (1995) 141-200.
[16] S. Ripperger and J. Altmann, Crossflow microfiltration – state of the art, Separat. Purif. Technol., 26 (2002) 19-31.
[17] D.R. Trettin and M.R. Doshi, Limiting flux in ultrafiltration of macromolecular solutions, Chem. Eng. Commun., 4 (1980) 507-522.
[18] A.L. Zydney and C.K. Colton, A concentration polarization model for filtrate flux in crossflow microfiltration of particulate suspensions, Chem. Eng. Commun., 47 (1986) 1-21.
[19] P. Harmant and P. Aimar, Coagulation of colloids in a boundary layer during crossflow filtration, Colloids Surf. A Physicochem. Eng. Aspects, 138 (1998) 217-230.
[20] Y. Ye, P. Le Clech, A.G. Fane and B. Jefferson, Fouling mechanisms of alginate solutions as model extracellular polymeric substances, Desalination, 175 (2005) 7-20.
[21] G. Genkin, T.D. Waite, A.G. Fane and S. Chang, The effect of vibration and coagulant addition on the filtration performance of submerged hollow fibre membranes, J. Membr. Sci., 281 (2006) 726-734.
[22] W.S. Guo, S. Vigneswaran and H.H. Ngo, Effect of flocculation and/or adsorption as pretreatment on the critical flux of crossflow microfiltration, Desalination, 172 (2005) 53-62.
[23] H.M. Huotari, I.H. Huisman and G. Tragardh, Electrically enhanced crossflow membrane filtration of oily waste water using the membrane as a cathode, J. Membr. Sci., 156 (1999) 49-60.
[24] F. Wang and V.V. Tarabara, Coupled effects of colloidal deposition and salt concentration polarization on reverse osmosis membrane performance, J. Membr. Sci., 293 (2007) 111-123.
[25] H.Y. Ng and M. Elimelech, Influence of colloidal fouling on rejection of trace organic contaminants by reverse osmosis, J. Membr. Sci., 244 (2004) 215-226.